Implementation of Modified Wheeler Model in Peridynamic Fatigue Model to Predict Effects of Overload and Underload on Fatigue Crack Growth Rate

Cong Tien Nguyen, Selda Oterkus, Erkan Oterkus*
PeriDynamics Research Centre (PDRC), Department of Naval Architecture, Ocean and Marine Engineering, University of Strathclyde, Glasgow, United Kingdom

Abstract

This study presents a novel peridynamic model for the prediction of fatigue crack growth rate with the effects of overload and underload. The modified Wheeler models for underload, overload and overload-underload combinations are applied to peridynamic fatigue equations. The capability of the proposed peridynamic fatigue model is demonstrated by considering fatigue crack growth on a single edge-notch plate subjected to constant amplitude loadings with overloads, underloads, and overload/underload combinations. The accuracy of the proposed peridynamic fatigue model is verified by comparing the predicted fatigue crack growth with experimental results.

Keywords: Peridynamics; fatigue; overload; underload; variable amplitude loading.

*Corresponding author: erkan.oterkus@strath.ac.uk

1. Introduction

Fatigue crack growth in many engineering structures generally involves variable amplitude or spectrum load rather than constant amplitude loading. It is well-known that overloads can cause retardation in which the fatigue crack growth rate is reduced. Therefore, the occurrence of overloads in a constant amplitude loading can extend the fatigue life for structures. On the other hand, the underloads can cause the acceleration for crack growth which can shorten the fatigue life of structures.

To consider the effects of overloads on fatigue crack growth, a model proposed by Wheeler [1], which is called the "Wheeler model" in later sections, has been widely used. In the Wheeler model, a correction factor, ϕ_R, was added to the original Paris' law equation as

$$\left(\frac{da}{dN}\right)_{VAL} = \phi_R \left(\frac{da}{dN}\right)_{CAL} \quad (1)$$

where $(da/dN)_{VAL}$ and $(da/dN)_{CAL}$ represent the fatigue crack growth due to variable amplitude loading and constant amplitude loading, respectively. The correction factor ϕ_R can be determined based on the crack length and plastic zone sizes due to overloads and the constant amplitude loading at the current cycle [1].

According to Wheeler [1], the crack growth rate is at its minimum immediately after the occurrence of the overload and gradually returns to its steady state in later stages as shown in Fig. 1(a). However, this assumption is not correct for materials that experience crack growth acceleration and delay retardation immediately after an overload as shown in Fig. 1(b) [2].

Determination of the correction factor ϕ_R requires a calibration of the shaping exponent by empirically fitting the variable amplitude loading test data and it generally depends on the material and the nature of the considered load spectrum. Therefore, different loading scenarios require the re-calibration of the shaping exponent. This leads to a requirement for a very large database of test data [3]. In addition, the original Wheeler model [1] can only model crack growth retardation due to single and periodic overloads. This model cannot deal with the effects of underloads and overload/underload combinations [4].

To improve the capability of the Wheeler model, many modified versions of this model have been proposed for different materials and load spectrums [2-14]. Yuen and Taheri [2] proposed a modified Wheeler model that can detailly consider three stages of the retardation process including accelerated crack growth, delay retardation, and the gradual returning to steady state. Moreover, the model proposed by Yuen and Taheri [2] can also consider the interaction between overloads. However, this model proposed several additional parameters which require additional calibrations for each single retardation stage. Huang, et al. [4] proposed an engineering model by using the equivalent stress intensity factor. The model was applicable to predict fatigue crack growth under variable amplitude loading for different materials. However, similar to the model in [2], the model proposed by Huang, et al. [4] requires more calibrations for additional parameters and shaping exponents. Mehrzadi and Taheri [7] proposed a simpler version of the modified Wheeler model by neglecting the accelerated crack growth process since this process is often very short and has little effect on the overall fatigue crack growth. This assumption gave a relatively good approximation for many different materials and various loading spectrums [7].

To avoid the requirement of calibrating shaping exponents in the Wheeler model, Willenborg, et al. [15] assumed the amount of retardation as a function of the stress intensity factor necessary to cancel the effect of the overload plastic zone. Therefore, the model proposed by Willenborg, et al. [15] does not require any empirical parameters. Instead, only the material yield stress is required. However, this model gives extremely overestimated predictions for high overload ratios ($R_{OL} > 1.6$) [3, 6].

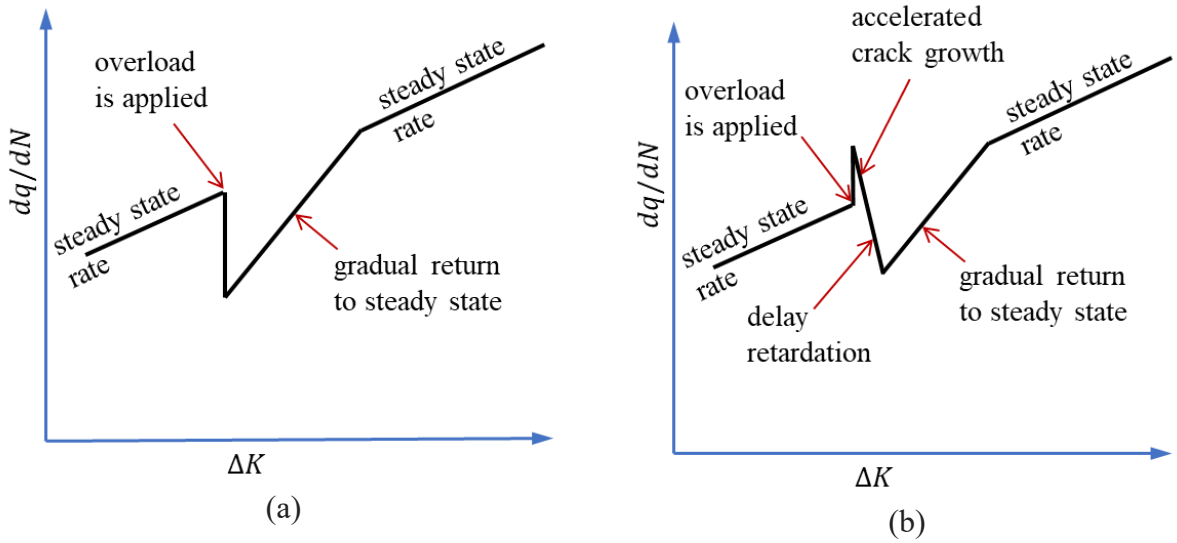

Fig. 1. Schematic crack growth curve with the retardation following an overload (a): without the acceleration and delay retardation according to the original Wheeler model, (b): with the acceleration and delay retardation.

To predict fatigue crack propagation, numerical methods such as the finite element method (FEM) by using the remeshing techniques [16, 17], or various modified versions of the FEM such as extended finite element method [18, 19], have been used. However, since the abovementioned methods are based on classical continuum mechanics (CCM) that use partial differential equations, additional criteria are needed to predict crack growth speed and direction or the branching of cracks [20-23].

Peridynamics (PD) is a reformulation of the CCM by using integro-differential equations instead of partial differential equations [24-26]. In PD, the behavior of a material point is influenced by its surrounding material points located within a finite distance δ which is called the horizon size. Since the integro-differential equations used in PD are valid in both continuous and discontinuous models, the PD theory is suitable for predicting progressive damages [27, 28].

The first PD models for fatigue cracking were developed by Oterkus, et al. [29] and Silling and Askari [30]. The fatigue model developed by Oterkus, et al. [29] degrades the critical bond stretch over fatigue cycles and it does not consider fatigue initiation. On the other hand, the model developed by Silling and Askari [30] can capture fatigue crack initiation (phase I), crack growth (phase II), and final failure controlled by quasi-static crack growth (phase III). Further validations for the PD fatigue model of Silling and Askari were studied by Zhang, et al. [31], Jung and Seok [32]. Recently, Nguyen, et al. [33] proposed an energy-based PD fatigue model using the cyclic

bond energy release rate range. Recently, Binchao, et al. [34] discussed the limitations of the PD fatigue model of Silling and Askari, and the authors developed a new fatigue damage-cumulative model in PD. The model developed by the authors can be applicable for both high cycle fatigue and low cycle fatigue problems, but it requires PD analysis of elastoplastic deformation to calculate elastic and plastic bond strains.

Compared to the PD fatigue model developed by Binchao, et al. [34], the PD fatigue model developed by Silling and Askari [30] is simpler, but it can only be applicable for constant amplitude loading and high cycle fatigue problems. Therefore, in this study, the implementation of the modified Wheeler model into the original PD fatigue model of Silling and Askari to consider overloading and underloading effects on the fatigue crack growth rate is proposed. The original PD fatigue equations for phase II proposed by Silling and Askari [30] are modified by adding the correction factor ϕ_R which can be determined based on the modified Wheeler model.

To demonstrate the capability of the proposed PD fatigue model, fatigue crack growths on a single edge-notch plate subjected to constant amplitude loadings with different overloads, underloads, and overload/underload combinations are predicted. The fatigue crack growths predicted by the proposed PD model are compared with experimental results.

This paper is organized as follows. Section 2 presents a brief review of the PD theory for 2D structures. Section 3 presents equations for the proposed PD fatigue model and the calculations of the correction factor ϕ_R for overloads, underloads, and overload-underload combinations. Section 4 provides the numerical implementation followed by the numerical results presented in Section 5. Finally, the conclusions are presented in Section 6.

2. Ordinary state-based peridynamic model

Peridynamics is a reformulation of continuum theory which is first introduced by Silling [24]. In PD, the motion of a material point is influenced by surrounding material points within a distance, δ, which is called horizon size. The material points located within the horizon δ of a material point are called the family members of that point. In PD, the motion of a material point is expressed in either the integro-differential or discrete equations as [26-28]

$$\rho(\mathbf{x})\ddot{\mathbf{u}}(\mathbf{x},t) = \int_{H_x} \psi(\mathbf{x}'-\mathbf{x},t)(\mathbf{t}(\mathbf{u}'-\mathbf{u},\mathbf{x}'-\mathbf{x},t) - \mathbf{t}'(\mathbf{u}-\mathbf{u}',\mathbf{x}-\mathbf{x}',t))dV' + \mathbf{b}(\mathbf{x},t) \quad (2a)$$

or

$$\rho_{(k)}\ddot{\mathbf{u}}_{(k)} = \sum_{j=1}^{N_k} \psi_{(k)(j)}\left(\mathbf{t}_{(k)(j)} - \mathbf{t}_{(j)(k)}\right)V_{(j)} + \mathbf{b}_{(k)} \quad (2b)$$

where ρ represents the mass density, $\mathbf{x}$ represents the vector of coordinates, $\ddot{\mathbf{u}}$ and $\mathbf{u}$ represent acceleration and displacement vectors, respectively. The parameter $\mathbf{b}$ represents the external body force density. The parameter H_x represents the horizon of the material point located at $\mathbf{x}$, and N_k represents the number of family members of the material point k. The term $V_{(j)}$ is the volume of the material point j which is a family member of the material point k. The term $\mathbf{t}_{(k)(j)}$ denotes the force density that the material point j exerts on the material point k and $\mathbf{t}_{(j)(k)}$ corresponds to the

force density that material point k exerts on the material point j. The parameter $\psi_{(k)(j)}$ determines whether the interaction is intact or broken which can be defined as [27]

$$\psi_{(k)(j)}\left(\mathbf{x}_{(j)}-\mathbf{x}_{(k)},t\right)=\begin{cases}1 & \text{if an interaction exists,}\\ 0 & \text{if no interaction.}\end{cases} \tag{3}$$

For linear elasticity, the linearized ordinary state-based PD equations of motion for a 2D structure can be represented as [26, 35, 36]

$$\rho h\ddot{u}_{(k)}=\sum_{j=1}^{N_k}\psi_{(k)(j)}\left[2ad\frac{1}{\xi}\left(\vartheta_{(k)}+\vartheta_{(j)}\right)+4bs_{(k)(j)}\right]cos\,\varphi\,V_{(j)}+\bar{b}_{x(k)} \tag{4a}$$

$$\rho h\ddot{v}_{(k)}=\sum_{j=1}^{N_k}\psi_{(k)(j)}\left[2ad\frac{1}{\xi}\left(\vartheta_{(k)}+\vartheta_{(j)}\right)+4bs_{(k)(j)}\right]sin\,\varphi\,V_{(j)}+\bar{b}_{y(k)} \tag{4b}$$

with

$$\vartheta_{(k)}=d\sum_{j=1}^{N_k}\psi_{(k)(j)}s_{(k)(j)}V_{(j)} \tag{4c}$$

$$s_{(k)(j)}=\frac{\left(u_{(j)}-u_{(k)}\right)cos\,\varphi+\left(v_{(j)}-v_{(k)}\right)sin\,\varphi}{\xi} \tag{4d}$$

$$cos\,\varphi=\frac{x_{(j)}-x_{(k)}}{\xi} \tag{4e}$$

$$sin\,\varphi=\frac{y_{(j)}-y_{(k)}}{\xi} \tag{4f}$$

$$\xi=\sqrt{\left(x_{(j)}-x_{(k)}\right)^2+\left(y_{(j)}-y_{(k)}\right)^2} \tag{4g}$$

$$a=\frac{1}{2}(\lambda\alpha-\mu) \tag{4h}$$

$$b=\frac{3E}{(1+\nu)\pi\delta^3} \tag{4i}$$

$$d=\frac{2}{\pi h\delta^2} \tag{4j}$$

In Eqs. (4a-b), $\bar{b}_{x(k)}$ and $\bar{b}_{y(k)}$ represent external forces per unit area and h represents the thickness of the 2D structure [36]. In Eqs. (4a-c), the term $\vartheta_{(k)}$ and $\vartheta_{(j)}$ represent the dilatations of material points k and j, respectively. The parameter $s_{(k)(j)}$ in Eq. (4d) represents the linearized bond stretch between material points k and j [26, 27, 36-38]. The parameter φ in Eqs. (4e-f) represents the angle between the line of interaction (between material points k and j in the undeformed configuration) and the x axis. The parameter ξ in Eq. (4g) represents the distance between material points k and j in the undeformed configuration. In Eq. (4a-b) and Eq. (4h-j), the terms a, b, d represent PD constants for 2D structures [36]. The terms λ and μ in Eq. (2h) represent the Lame's constants which can be defined as

$$\lambda = \frac{E\nu}{(1+\nu)(1-2\nu)};\ \ \mu = \frac{E}{2(1+\nu)} \tag{5}$$

where E and ν represent the elastic modulus and Poisson's ratio, respectively.

To determine the state of interaction in PD, two main damage criteria, which are critical stretch [26-28] and critical energy release rate [36, 39-43], are commonly used. The damage criteria based on the critical stretch can be described as [26-28]

$$\begin{cases} s_{(k)(j)} < s_c \rightarrow \text{interaction exists: } \psi_{(k)(j)} = 1 \\ s_{(k)(j)} \geq s_c \rightarrow \text{interaction is broken: } \psi_{(k)(j)} = 0 \end{cases} \tag{6}$$

where s_c represents the critical stretch. For 2D structures, the critical stretch can be calculated as [27, 28]

$$s_c = \sqrt{\frac{G_c}{\left(\frac{6}{\pi}\mu + \frac{16}{9\pi^2}(\kappa - 2\mu)\right)\delta}} \tag{7}$$

where G_c represents the critical energy release rate of material, and κ represents the bulk modulus of the material.

To represent the local damages on the structure, the damage index, ϕ is used. This damage index is the ratio of broken interactions to the total number of interactions within the horizon of a material point, which can be represented as [27]

$$\phi\left(\mathbf{x}_{(k)}, t\right) = 1 - \frac{\sum_{j=1}^{N_k} \psi_{(k)(j)}\left(\mathbf{x}_{(j)} - \mathbf{x}_{(k)}, t\right) V_{(j)}}{\sum_{j=1}^{N} V_{(j)}} \tag{8}$$

For static loading conditions, the terms related to inertia forces on the left-hand side of Eq. (4a, b) are neglected. Therefore, Eq. (4a, b) can be rewritten as

$$-\sum_{j=1}^{N_k} \psi_{(k)(j)} \left[2ad\frac{1}{\xi}\left(\vartheta_{(k)} + \vartheta_{(j)}\right) + 4bs_{(k)(j)}\right] cos\,\varphi\, V_{(j)} = \bar{b}_{x(k)} \tag{9a}$$

$$-\sum_{j=1}^{N_k} \psi_{(k)(j)} \left[2ad\frac{1}{\xi}\left(\vartheta_{(k)} + \vartheta_{(j)}\right) + 4bs_{(k)(j)}\right] sin\,\varphi\, V_{(j)} = \bar{b}_{y(k)} \tag{9b}$$

In Eqs. (4a, b) and Eqs. (9a, b), the external loading is applied as forces per unit area. To apply the external loading as forces, Eq. (9) can be modified by multiplying both sides with the area of material point $A_{(k)}$ as

$$-A_{(k)}\sum_{j=1}^{N_k} \psi_{(k)(j)} \left[2ad\frac{1}{\xi}\left(\vartheta_{(k)} + \vartheta_{(j)}\right) + 4bs_{(k)(j)}\right] cos\,\varphi\, V_{(j)} = F_{x(k)} \tag{10a}$$

$$-A_{(k)}\sum_{j=1}^{N_k} \psi_{(k)(j)} \left[2ad\frac{1}{\xi}\left(\vartheta_{(k)} + \vartheta_{(j)}\right) + 4bs_{(k)(j)}\right] sin\,\varphi\, V_{(j)} = F_{y(k)} \tag{10b}$$

3. Peridynamic fatigue model for variable amplitude loading

In this section, first, the PD fatigue equations for variable amplitude loading are presented in Section 3.1. To consider the effects of overloads and underloads, the retardation factor, ϕ_R is added to the original PD fatigue equations proposed by Silling and Askari [30]. Later, the modified Wheeler models to determine the retardation factor, ϕ_R for overloads, underloads, and overload-underload combinations are proposed in Section 3.2, 3.3, and 3.4, respectively.

3.1. Peridynamic fatigue equations for fatigue crack growth

In PD, the fatigue life of each interaction (bond) is represented by the remaining life, λ, which can be reduced from 1 to 0 due to fatigue cyclic loading. The remaining life of $0 < \lambda \leq 1$ means that the bond is still intact. Meanwhile, the fatigue life of $\lambda = 0$ means that the bond is broken.

The original PD fatigue model proposed by Silling and Askari [30] includes equations for fatigue crack initiation (phase I) and fatigue crack growth (phase II). The fatigue equation for phase I is based on the $\varepsilon - N$ curve. Meanwhile, the fatigue equation for phase II is based on the $da/dN - \Delta K$ curve in the Paris' law.

For phase II fatigue equation, Silling and Askari [30] proposed the following equation for constant amplitude loading as

$$\lambda_{(k)(j)}^{(N=0)} = 1, \left(\frac{d\lambda_{(k)(j)}^{(N)}}{dN}\right)_{CA} = -A_2\left(\varepsilon_{(k)(j)}^{(N)}\right)^{m_2} \text{ with } A_2 > 0, m_2 > 0 \tag{11a}$$

with

$$\varepsilon_{(k)(j)}^{(N)} = \left|s_{(k)(j)}^{(N+)} - s_{(k)(j)}^{(N-)}\right| = \left|s_{(k)(j)}^{(N+)}(1-R)\right| \tag{11b}$$

and

$$R = \frac{P_{min}}{P_{max}} = \frac{s_{(k)(j)}^{(N-)}}{s_{(k)(j)}^{(N+)}} \tag{11c}$$

where $\lambda_{(k)(j)}^{(N=0)}$ represents the initial fatigue life of the interaction between material points k and j. The parameters $\lambda_{(k)(j)}^{(N)}$ and $\varepsilon_{(k)(j)}^{(N)}$ represent the fatigue life and cyclic bond strain range of this interaction at N^{th} cycle. The parameters $s_{(k)(j)}^{(N+)}$ and $s_{(k)(j)}^{(N-)}$ are bond stretches corresponding to maximum loading, P_{max}, and minimum loading, P_{min}, at N^{th} cycle. The parameter R represents the loading ratio.

In Eq. (11a), parameters A_2 and m_2 are fatigue parameters for phase II which need to be calibrated. The parameter m_2 can be obtained based on the Paris' law equation of material as

$$dq/dN = C\Delta K^M \tag{12a}$$

$$m_2 = M \tag{12b}$$

Meanwhile, the parameter A_2 can be obtained by conducting a trial PD fatigue simulation for a constant amplitude loading case [30]. Specifically, a trial value $A_{2(trial)}$ is assumed and a trial PD fatigue simulation with fatigue parameters of $\left(A_{2(trial)}, m_2\right)$ is conducted. From this trial

simulation, the fatigue crack growth rate $(dq/dN)_{(trial)}$ and the SIF range ΔK are calculated [30, 31, 33]. Next, the calculated values for $(dq/dN)_{(\text{trial})}$ and ΔK are assumed to follow the Paris' law equation $(dq/dN)_{(trial)} = C_{(trial)}\Delta K^M$, and the best-fit value for $C_{(trial)}$ is obtained. Therefore, by comparing the equation $(dq/dN)_{(trial)} = C_{(trial)}\Delta K^M$ with the real Paris' law equation of material given in Eq. (12a), the fatigue parameter A_2 can be obtained as [30, 33]

$$A_2 = A_{2(trial)} \frac{C\Delta K^M}{C_{(trial)}\Delta K^M} = A_{2(trial)} \frac{C}{C_{(trial)}} \tag{13}$$

As given in Eq. (11), the PD fatigue equation for phase II proposed by Silling and Askari [30] is applicable for constant amplitude loading. When the structure is subjected to variable amplitude loading, the sudden changes of loading amplitudes can cause retardation effects which can change the fatigue crack growth significantly. To consider the effects of overloads and underloads on the fatigue crack growth, a retardation factor, ϕ_R, can be added to the original Paris's law equation as [1, 2, 5-7]

$$\left(\frac{dq}{dN}\right)_{VAL} = \phi_R \left(\frac{dq}{dN}\right)_{CAL} = \phi_R (C\Delta K^m) \tag{14}$$

Therefore, in this study, to consider the effects of overloads and underloads, the retardation factor, ϕ_R is added to the original phase II PD fatigue equation given in Eq. (11) as

$$\lambda_{(k)(j)}^{(N=0)} = 1, \left(\frac{d\lambda_{(k)(j)}^{(N)}}{dN}\right)_{VA} = \phi_R \left(\frac{d\lambda_{(k)(j)}^{(N)}}{dN}\right)_{CA} \tag{15a}$$

or

$$\lambda_{(k)(j)}^{(N=0)} = 1, \left(\frac{d\lambda_{(k)(j)}^{(N)}}{dN}\right)_{VA} = -\phi_R A_2 \left(\varepsilon_{(k)(j)}^{(N)}\right)^{m_2} \text{ with } A_2 > 0, m_2 > 0 \tag{15b}$$

where ϕ_R is the retardation factor which represents the effects of overloads and underloads. For constant amplitude loading, $\phi_R = 1$. The formulations of ϕ_R to consider effects of overloads, underloads, and overload-underload combinations are presented in Section 3.2, 3.3, and 3.4, respectively.

By using the relation given in Eq. (15b), the remaining life of a bond in phase II can be updated as

$$\lambda_{(k)(j)}^{(N=0)} = 1, \lambda_{(k)(j)}^{(N)} = \lambda_{(k)(j)}^{(N-1)} - \phi_R A_2 \left(\varepsilon_{(k)(j)}^{(N)}\right)^{m_2} \tag{16}$$

Beyond the crack growth phase (phase II), the structures can experience rapid crack growth (phase III). In this case, the traditional PD model [25-28] for damage prediction can be used. Therefore, the interaction state of a bond can be defined as

$$\begin{cases} \lambda_{(k)(j)}^{(N)} \leq 0 \quad \text{or} \quad s_{(k)(j)} \geq s_c \;\rightarrow\; \psi_{(k)(j)} = 0 \\ \lambda_{(k)(j)}^{(N)} > 0 \quad \text{and} \quad s_{(k)(j)} < s_c \;\rightarrow\; \psi_{(k)(j)} = 1 \end{cases} \tag{17}$$

3.2. Overloading effects

In this section, the calculation for the retardation factor, ϕ_R due to overloads is presented. As proposed by Yuen and Taheri [2], the retardation process can have three main stages, including accelerated crack growth, delay retardation, and gradual returning to the steady state. For many materials, the accelerated crack growth processes are often very short, and it has insignificant effects on the overall fatigue crack growth [2, 4, 7]. Therefore, the effect of the accelerated crack growth process is neglected in this study. Thus, the retardation process due to a single overload is assumed to have two main stages including the delay retardation process and gradual returning to steady state as shown in Fig. 2.

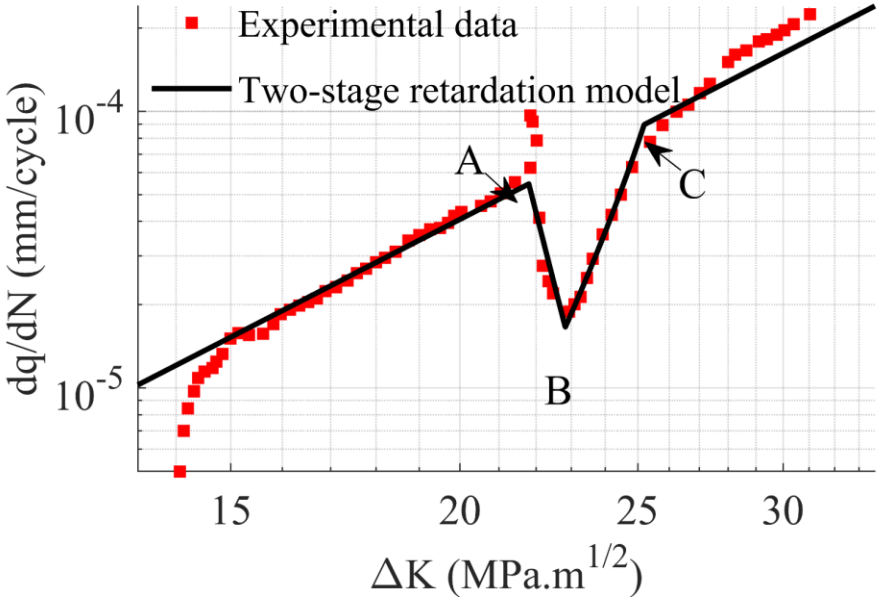

Fig. 2. Schematic for two-stage retardation model

In Fig. 2, point A corresponds to the moment that the overload is applied. Point B corresponds to the end of the delay retardation process and point C is where the fatigue crack growth is completely returning to the steady state of the crack growth under constant amplitude loading. The period from point A to point B is the delay retardation process. Meanwhile, the period from point B to point C is the process of the fatigue crack growth gradually returning to the steady state. This two-stage retardation process was proposed by Mehrzadi and Taheri [7]. According to Mehrzadi and Taheri [7], the value of the coefficient ϕ_R for a single overload can be calculated as

$$\phi_R = \begin{cases} (\phi_{Rd})^{\frac{q_i - q_{OL}}{q_d - q_{OL}}} & \text{if} \quad q_{OL} \le q_i < q_d \\ \left[\frac{r_i}{q_{OL} + \beta r_{OL} - q_i}\right]^n & \text{if} \quad q_d \le q_i < q_{OL} + \beta r_{OL} - r_i \\ 1 & \text{otherwise} \end{cases} \tag{18}$$

where β and n are two coefficients that need to be determined based on best fitting with experimental data for the $dq/dN - \Delta K$ curve. The parameter q_{OL} represents the crack length at which the overload is applied. Meanwhile, q_i represents the current crack length at the i^{th} loading cycle. The parameter r_{OL} represents the plastic zone size due to the overload and r_i represents the current effective plastic zone size at q_i . These plastic zone sizes can be estimated as [4, 44]

$$r_{OL} = \alpha_{OL}\left(\frac{K_{OL}}{\sigma_y}\right)^2 \tag{19a}$$

$$r_i = \alpha_i\left(\frac{K_i}{\sigma_y}\right)^2 \tag{19b}$$

with

$$\alpha_{OL} = 0.35 - \frac{0.29}{1+\left[1.08K_{OL}^2/(h\sigma_y^2)\right]^{2.15}} \tag{19c}$$

$$\alpha_i = 0.35 - \frac{0.29}{1+\left[1.08K_i^2/(h\sigma_y^2)\right]^{2.15}} \tag{19d}$$

In Eq. (19), K_{OL} is the stress intensity factor corresponding to the overload P_{OL}, and K_i is the stress intensity factor corresponding to the load P_{max} at the current i^{th} loading cycle. The term σ_y represents the yield strength of the material, α_{OL} and α_i represent the plastic zone size factors for overload P_{OL} and current loading P_{max}. The formulations for plastic zone size factors given in Eqs. (19c-d) were proposed by Huang, et al. [4]. This formulation for the plastic zone size factor gives very close values to those obtained by using other well-known formulations proposed by Irwin [44], Guo [45], Voorwald, et al. [46].

In Eq. (18), the parameter q_d represents the crack length at the end of the delay retardation process which corresponds to point B in Fig. 2. Mehrzadi and Taheri [7] and Yuen and Taheri [2] determined the values of q_d based on experimental data. It means that q_d is required to be recalibrated for different loading spectrum corresponding to different values of R, R_{OL} and r_{OL}.

In this study, to avoid the recalibration of q_d for each new loading spectrum, q_d is proposed to have some relations with the plastic zone size due to the overload, r_{OL}, crack length at the occurrence of overload, q_{OL}, the loading ratio R and the overloading ratio R_{OL} as

$$\frac{q_d - q_{OL}}{r_{OL}} = f(R, R_{OL}) \tag{20a}$$

or

$$q_d = q_{OL} + r_{OL} f(R, R_{OL}) \tag{20b}$$

where R_{OL} represents the overloading ratio R_{OL} which can be defined as

$$R_{OL} = P_{OL}/P_{max} \tag{21}$$

In Eqs. (20a, b), $f(R, R_{OL})$ is a function of loading ratio R and overloading ratio R_{OL} that needs to be determined. In this study, $f(R, R_{OL})$ is determined by using linear regression of the experimental data. Details of the determination of $f(R, R_{OL})$ and q_d are presented in Appendix A1.

In Eq. (18), the parameter ϕ_{Rd} represents the value of ϕ_R at the end of the delay retardation process which corresponds to point B in Fig. 2. In this study, the parameters q_d, ϕ_{Rd}, β, and n for the proposed model given in Eq. (18) are determined by using two-step calibrations as presented in Appendix A.

3.3. Underloading effects

After the occurrence of an underload, the crack growth speed is increased in a short period, and the constant amplitude growth rate is restored quickly. Similar to the formulation proposed in [13], when underload is independently exerted in the constant amplitude baseline loading, the coefficient ϕ_R can be estimated as

$$\phi_R = \begin{cases} \left[\frac{\beta\, r_{UL}}{q_i + r_i - q_{UL}}\right]^n & \text{if} \quad q_{UL} \le q_i \le q_{UL} + \beta r_{UL} - r_i \\ 1 & \text{if} \quad q_i + r_i > q_{UL} + \beta r_{UL} \end{cases} \tag{22}$$

where q_{UL} represents the crack length at which the underload is applied, q_i is the current crack length at the i^{th} loading cycle, and r_i is the current plastic zone size due to the i^{th} loading cycle. The parameter r_{UL} represents the plastic zone created by the underload which can be estimated as [4]

$$r_{UL} = \alpha_{UL}\left(\frac{\Delta K_{min,UL}}{\sigma_Y}\right)^2 = \alpha_{UL}\left(\frac{K_{min,CAL} - K_{\min,UL}}{\sigma_Y}\right)^2 \tag{23a}$$

with

$$\Delta K_{min,UL} = K_{min,CAL} - K_{\min,UL} \tag{23b}$$

and

$$\alpha_{UL} = 0.35 - \frac{0.29}{1 + \left[\frac{1.08\left(K_{min,CAL} - K_{\min,UL}\right)^2}{h\sigma_y^2}\right]^{2.15}} \tag{23c}$$

where $K_{min,CAL}$ and $K_{\min,UL}$ represent the stress intensity factors corresponding to the minimum load P_{min} and the underload P_{UL}, respectively.

In Eq. (22), (β, n) are the coefficients that need to be determined based on best-fit results with experimental data. The detailed calibrations for parameters (β, n) for underload are presented in Appendix B.

3.4. Combined effects of overloads and underloads

The modified models presented in Sections 3.2 and 3.3 can predict the crack growth retardation or acceleration due to the independent application of single and multiple overloads or underloads. However, these models cannot deal with the effects of the combination of overloads and underloads. If an underload is applied immediately after an overload, the degree of retardation due to the overload is reduced but not eliminated. On the other hand, if an underload is applied before an overload, the underload has little effect on the degree of crack retardation due to the overload [3, 4]. In this section, a modified Wheeler model for the combinations of overloads and underloads is proposed. The value of ϕ_R for either overload/underload or underload/overload is calculated as

$$\phi_R = \phi_{R,OL} \times \phi_{R,UL} \tag{24}$$

where $\phi_{R,UL}$ is an estimated value for ϕ_R caused by underloads by using the proposed model in Eqs. (26-27) in Section 3.3. Meanwhile, $\phi_{R,OL}$ is an estimated value for ϕ_R caused by overloads.

At the moment that overload is applied, if the crack growth rate is at the steady state of constant amplitude loading, $\phi_{R,OL}$ can be calculated by using the model given in Eq. (18) in Section 3.2. However, there are some cases that the overload is applied when the effects of the previous overloads or underloads are still existing. In those cases, the crack growth rate is not at a steady state when the overload is applied. Therefore, $\phi_{R,OL}$ can be calculated by modifying Eq. (18) as

$$\phi_{R,OL} = \begin{cases} (\bar{\phi}_R)^{\left(\frac{q_d - q_i}{q_d - q_{OL}}\right)} (\phi_{Rd})^{\frac{q_i - q_{OL}}{q_d - q_{OL}}} & \text{if} \quad q_{OL} \le q_i < q_d \\ \left[\frac{r_i}{q_{OL} + \beta r_{OL} - q_i}\right]^n & \text{if} \quad q_d \le q_i < q_{OL} + \beta r_{OL} - r_i \\ 1 & \text{otherwise} \end{cases} \tag{25}$$

In Eq. (25), the term $(\bar{\phi}_R)^{\left(\frac{q_d - q_i}{q_d - q_{OL}}\right)}$ represents the existing effects of the previous overloads or underloads on the current overload. The parameter $\bar{\phi}_R$ represents the value of ϕ_R when the current overload is applied. If the current overload is exerted in the constant amplitude baseline loading, $\bar{\phi}_R = 1$. Therefore, the model given in Eq. (25) reduces to the overloading model given in Eq. (18). If the current overload is exerted within the existing effects of previous overloads or underloads, $\bar{\phi}_R$ can differ to 1.

4. Numerical Implementation

In the PD model, the domain is uniformly discretized with material points associated with specific volumes. For each cycle, to update the fatigue life of each interaction, the displacement field of the structure subjected to the static loading $P = P_{max}$ is obtained by solving equations given in Eq. (10). In this study, the direct stiffness method proposed by Nguyen, et al. [33] for static loading conditions is used to obtain the displacement field of the structure. Next, the bond stretch, $s_{(k)(j)}^{(N+)}$, and cyclic bond strain range, $\varepsilon_{(k)(j)}^{(N)}$, for each interaction are calculated by using Eq. (4d) and Eq. (11b), respectively. The remaining life of each interaction is updated by using Eq. (16) for phase II.

At each cycle, if there is no new broken bond in the PD model, the stiffness matrix of the structure will remain the same as the previous cycle. Therefore, under the same value of loading P_{max}, the displacement field, bond stretches, and cyclic bond strain ranges will remain the same as the previous cycle. As a result, the static solution for the current cycle can be skipped and the values of displacement and cyclic bond strain range from the previous cycle can be used to update fatigue life for interactions at the current cycle.

To determine whether there are new broken bonds or not, the summation of all interaction states is compared with its value in the previous load cycle [33]. The summation of all interaction states at the current cycle and previous cycle can be represented as

$$\Pi^{(n)} = \sum_{k=1}^{m} \sum_{j=1}^{N_k} \psi_{(k)(j)}^{(n)} \tag{26a}$$

$$\Pi^{(n-1)} = \sum_{k=1}^{m} \sum_{j=1}^{N_k} \psi_{(k)(j)}^{(n-1)} \tag{26b}$$

where $\Pi^{(n)}$ is the summation of all interaction states at n^{th} cycle, $\Pi^{(n-1)}$ is the summation of all interaction states at $(n-1)^{th}$ cycle. The parameter $\psi_{(k)(j)}^{(n)}$ represents the interaction state of the bond between material points k and j at n^{th} cycle and $\psi_{(k)(j)}^{(n-1)}$ represents the interaction state of the bond between material points k and j at $(n-1)^{th}$ cycle.

If the summation of all interaction states at the current cycle is smaller than its value at the previous cycle, $\Pi^{(n)} < \Pi^{(n-1)}$, it means that some new bonds are broken. Therefore, the static solution for extreme loading $P = P_{max}$ needs to be solved to obtain a new displacement field. Otherwise, there is no newly broken bond in the PD model and the static solution can be skipped. Therefore, the solution results for the $(n-1)^{th}$ cycle can be used for the n^{th} cycle.

After obtaining displacement field caused by the extreme loading $P = P_{max}$, the bond stretch and cyclic bond strain range for each interaction is calculated by using Eq. (4d) and Eq. (11b), respectively. If in the PD model, there is at least one interaction with bond stretch higher than the critical bond stretch, s_c, the PD model for phase III given in Section 2 is applied. On the other hand, the remaining life of each interaction is updated by using Eq. (16) for phase (II).

If the loading amplitude is a constant, the coefficient ϕ_R in Eq. (16) is equal to 1. If an overload occurs, the coefficient ϕ_R in Eq. (16) is calculated by using Eqs. (18-20) in Section 3.2. If an underload occurs, the coefficient ϕ_R in Eq. (16) is calculated by using Eqs. (22-23) in Section 3.3. If a combination of overloads and underloads occurs, the coefficient ϕ_R in Eq. (16) is calculated by using Eqs. (24-25) in Section 3.4.

After updating the fatigue life, the state of each interaction is updated by using Eq. (17), and the damage index ϕ for each material point is updated by using Eq. (8).

5. Numerical examples

In this section, first, the proposed PD fatigue model is used to predict the fatigue crack growth on a single edge-notch plate subjected to constant amplitude loading as presented in Section 5.1. Next, the fatigue crack growth for different loading scenarios of single overloads exerting in the constant amplitude baseline loading is presented in Section 5.2. Finally, the fatigue crack growth for different loading scenarios of a single underload, overload/underload, and underload/overload exerting in the constant amplitude baseline loading are presented in Section 5.3.

5.1. Constant amplitude loading

In this section, fatigue crack growth on a single edge-notch plate subjected to a constant amplitude loading is considered as shown in Fig. 3. The structure is made of Q345R steel with the elastic modulus of $E = 2.125 \times 10^{11}$ N/m^2 and Poisson's ratio of $\nu = 0.31$ [47, 48]. The dimensions of the plate are shown in Fig. 3(a) and the PD discretized model is shown in Fig. 3(b). The thickness of the plate is 3.8 mm and the initial crack length is $q_n = 10$ mm. The plate is subjected to cyclic loading with a constant amplitude of $P_{max} = 3.0$ kN and a load ratio of $R = 0.1$ [47].

In PD, the model is uniformly discretized with a mesh size of $\Delta x = W/150$ and the horizon size of $\delta = 3.015\Delta x$ is used. Since the problem is symmetric, the fixed boundary conditions at two

material points located at $(L_x, \Delta x/2)$ and $(L_x, -\Delta x/2)$, shown in pink in Fig. 3(b), are assumed to avoid rigid body motions in the PD simulation. To apply loading conditions, material points located inside the cut-outs, shown in cyan in Fig. 3(b), are assumed as rigid with the elastic modulus of $E_{rigid} = 200E$. Meanwhile, the load $P_{max} = 3.0$ kN is applied to the material points located at the centers of the cut-outs as shown in red in Fig. 3(b).

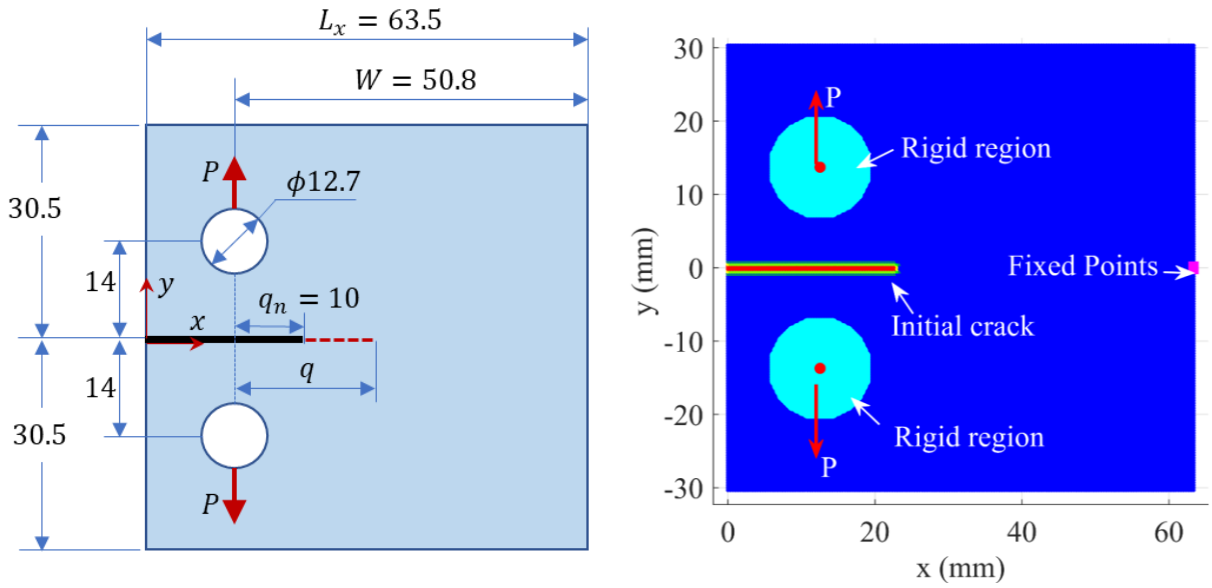

(a) (b)

Fig. 3. A single edge-notch plate subjected to a constant amplitude loading (a) geometry (dimensions are in mm), (b): PD discretized model (dimensions are in mm)

The fatigue parameter $m_2 = 3.41$ for phase II is obtained from the Paris' law equation $dq/dN = 1.49 \times 10^{-9}\Delta K^{3.41}$ mm/cycle given by Ding, et al. [47]. To determine fatigue parameter A_2, first, a trial value $A_{2(trial)} = 5 \times 10^4$ is assumed. Next, a trial PD fatigue simulation using $(A_{2(trial)}, m_2)$ is conducted to calculate the fatigue crack growth rate $(dq/dN)_{(\text{trial})}$ and the stress intensity factor range ΔK [30, 31, 33]. The results for $(dq/dN)_{(\text{trial})} - \Delta K$ curve obtained from the trial PD fatigue simulation is presented in Fig. 4(a). As shown in Fig. 4(a), the best-fit Paris' law equation can be obtained from this trial PD simulation as

$$(dq/dN)_{(\text{trial})} = C_{(\text{trial})}\Delta K^{3.41} \quad \text{with} \quad C_{(\text{trial})} = 8.3324 \times 10^{-10} \tag{27}$$

Therefore, the fatigue parameter A_2 can be obtained by using Eq. (13) as [30, 33]

$$A_2 = A_{2(trial)}\frac{C}{C_{(trial)}} = 50000\frac{1.49\times10^{-9}}{8.3324\times10^{-10}} = 89410 \tag{28}$$

Fig. 4 shows the predicted fatigue crack growth $dq/dN - \Delta K$ curve in PD simulations by using $A_{2(trial)} = 5 \times 10^4$ and $A_2 = 89410$. As shown in Fig. 4(a) for the trial simulation $A_{2(trial)} = 5 \times 10^4$, the predicted $(dq/dN)_{(\text{trial})} - \Delta K$ curve is significantly deviated from the experimental

equation. However, with the calibrated value $A_2 = 89410$, the predicted $dq/dN - \Delta K$ curve matched well with the experimental equation as shown in Fig. 4(b).

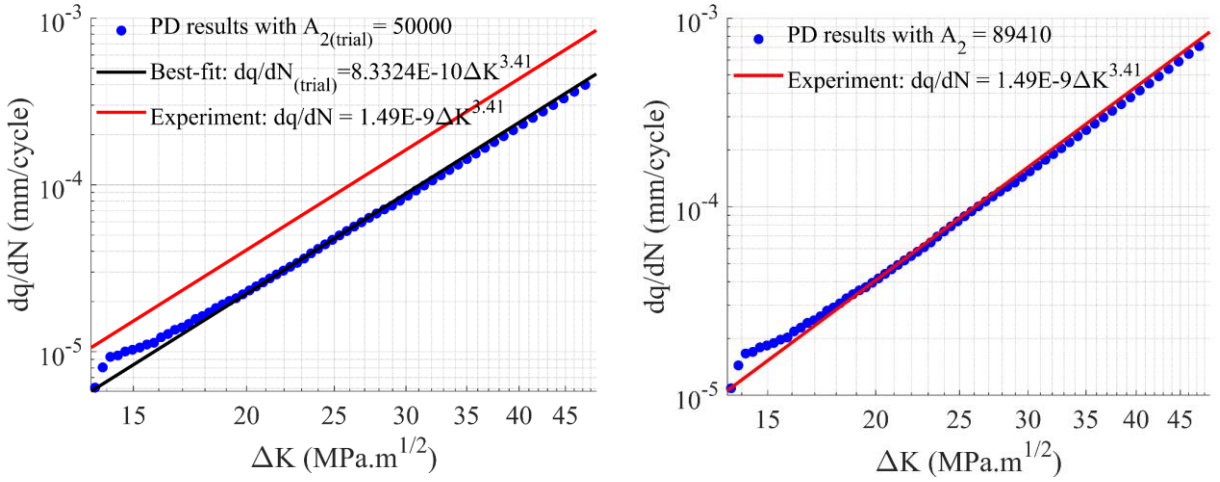

Fig. 4. Fatigue crack growth $dq/dN - \Delta K$ curves obtained from (a) the trial PD simulation with $A_{2(trial)} = 5 \times 10^4$, (b) the PD simulation with $A_2 = 89410$

Fig. 5 shows the fatigue crack propagation on the plate predicted by the PD model with $A_2 = 89410$, and $m_2 = 3.41$. As shown in Fig. 5(a), at the first loading cycle, the crack tip location is at $x \approx 22.7$ mm corresponding to the initial crack length of $q_n \approx 10$ mm. When the cyclic loading is continuously applied, the crack propagates along x direction which agrees with the experimental observation in Ding, et al. [47], [48]. After 456413 loading cycles, the crack tip location is at $x \approx 37.25$ mm and the crack length is $q \approx 27.25$ mm as shown in Fig. 5(b). For demonstration purposes, the displacements of material points are magnified by 40 for deformed configurations.

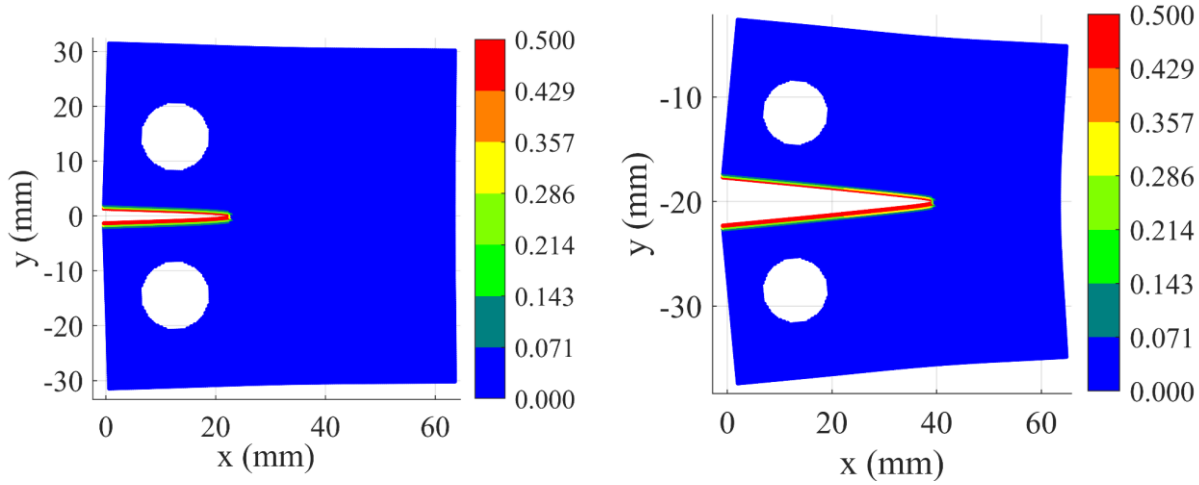

Fig. 5. Fatigue damage evolution under constant amplitude loading at (a) the first cycle when $q \approx 10$ mm, (b) 456413^{th} cycles when $q \approx 27.25$ mm (displacements are magnified by 40 for deformed configurations)

5.2. Single overload

In this section, the proposed PD model is used to predict effects on the fatigue crack growth of different overloads exerting in constant amplitude loadings. Details of investigated loading scenarios are shown in Table 1. In Table 1, specimens DJ02 and DJ11 have the same constant amplitude loading with $P_{max} = 3.0$ kN and $R = 0.1$. However, they have different overloading ratios R_{OL} of 1.5 and 2.0, respectively. Specimens DJ10 and DJ19 have the same constant amplitude loading with $P_{max} = 5.0$ kN and $R = 0.5$, but they have different overloading ratios R_{OL} of 1.5 and 2.0, respectively. Meanwhile, specimen DJ08 has a constant amplitude loading with $P_{max} = 3.0$ kN, $R = 0.2$ and an overloading ratio R_{OL} of 2.0. For all specimens, overloads are applied one time when the stress intensity factor range is at $\Delta K = \Delta K_{OL} = 21.80$ MPa$\sqrt{\text{m}}$. All specimens have the same geometrical and material properties as given in Section 5.1. The material has a yield strength of $\sigma_y = 324.4 \times 10^6$ N/m^2 [49].

Table 1. Different cases of constant amplitude loading with single overload.

Specimen	P_{max} (kN)	R	P_{OL} (kN)	R_{OL}	ΔK_{OL} (MPa$\sqrt{\text{m}}$)
DJ02	3.0	0.1	4.5	1.5	21.80
DJ08	3.0	0.2	6.0	2.0	21.80
DJ10	5.0	0.5	7.5	1.5	21.80
DJ11	3.0	0.1	6.0	2.0	21.80
DJ19	5.0	0.5	10.0	2.0	21.80

To utilize the PD model proposed in Section 3.1 for predicting overloading effects, the crack length at the end of the delay retardation process, q_d, the value of ϕ_R at the end of the delay retardation process, ϕ_{Rd}, and the coefficients (β, n) for the modified Wheeler model presented in Section 3.2 need to be determined. Details of the calibration for q_d, ϕ_{Rd}, β and n for all specimens are presented in Appendix A. The obtained values for q_d, ϕ_{Rd}, and (β, n) for all specimens are presented in Table 2.

Table 2. Values for q_d and (β, n) for different single overloading cases

Specimen	P_{max} (kN)	R	P_{OL} (kN)	R_{OL}	ΔK_{OL} (MPa$\sqrt{\text{m}}$)	q_{OL} (m)	q_d (m)	β	n	ϕ_{Rd}
DJ02	3.0	0.1	4.5	1.5	21.80	0.0193	0.0202	1.20	1.55	0.2601
DJ08	3.0	0.2	6.0	2.0	21.80	0.0216	0.0228	1.20	1.85	0.0685
DJ10	5.0	0.5	7.5	1.5	21.80	0.0208	0.0213	1.00	0.90	0.5140
DJ11	3.0	0.1	6.0	2.0	21.80	0.0193	0.0210	1.50	1.90	0.0445
DJ19	5.0	0.5	10.0	2.0	21.80	0.0208	0.0217	0.60	1.50	0.3300

Fig. 6 and Fig. 7 show the predicted fatigue crack growth for DJ02 and DJ11 specimens, respectively. The experimental data, shown in blue, is obtained from the study by Ding, et al. [47]. Here, the DJ02 specimen is subjected to loading with $P_{max} = 3.0$ kN, $R = 0.1$ and $R_{OL} = 1.5$. Meanwhile, the DJ11 specimen is subjected to loading with $P_{max} = 3.0$ kN, $R = 0.1$ and $R_{OL} = 2.0$.

For specimen DJ02, the overload of $P_{OL} = 4.5$ kN was applied when the crack length was approximately $q_{OL} \approx 19.3$ mm. As shown in Fig. 6(a), after the overload was applied, the $q - N$

curve of specimen DJ02 was changed significantly due to the reduction of fatigue crack growth rate. Moreover, the predicted $q-N$ curve for specimen DJ02 agrees very well with the experimental results.

As shown in Fig. 6(b) for the $dq/dN-\Delta K$ curve, there is also a good agreement between the predicted and experimental results. As can be observed from the experimental data in Fig. 6(b), at the beginning of the fatigue crack propagation when $\Delta K < 16\ \mathrm{MPa}\sqrt{\mathrm{m}}$, there were some effects of the fatigue threshold on the fatigue crack growth. However, these effects are not considered in the current PD model. Therefore, there is a slight difference in the fatigue crack growth rate at the beginning of the crack propagation process. In addition, at the end of the fatigue crack growth when $\Delta K \geq 26\ \mathrm{MPa}\sqrt{\mathrm{m}}$, the experimental fatigue crack growth rate are higher than the values obtained by using the Paris' law equation of $dq/dN = 1.49\times10^{-9}\Delta K^{3.41}$ mm/cycle proposed by Ding, et al. [47] as shown in Fig. 6(b). Since the PD model is calibrated based on this Paris' law equation, there is also a slight difference between the predicted and the experimental values of the fatigue crack growth rate at the end of the crack propagation process.

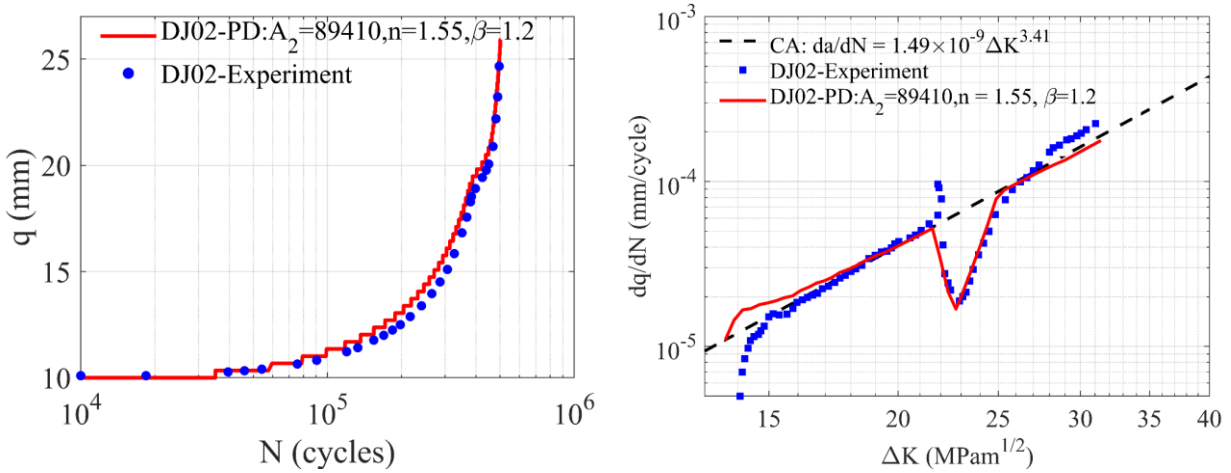

(a) (b)

Fig. 6. Fatigue crack growth on specimen DJ02 (a): $q-N$ curve, (b): $dq/dN-\Delta K$ curve

Fig. 7 shows the predicted fatigue crack growth for DJ11 specimen. The overload of $P_{OL} = 6.0$ kN was applied when the crack length was approximately $q_{OL} \approx 19.3$ mm. As shown in Fig. 7(b), after the overload was applied, the crack growth rate dq/dN reduced significantly to around 4.5×10^{-6} mm/cycle. Moreover, the $dq/dN-\Delta K$ curve predicted by using the PD fatigue model also agrees well with the experimental results. As shown in Fig. 7(a), the $q-N$ curve for specimen DJ11 was changed significantly due to the reduction of fatigue crack growth rate. The predicted $q-N$ curve for specimen DJ11 agrees very well with the experimental results.

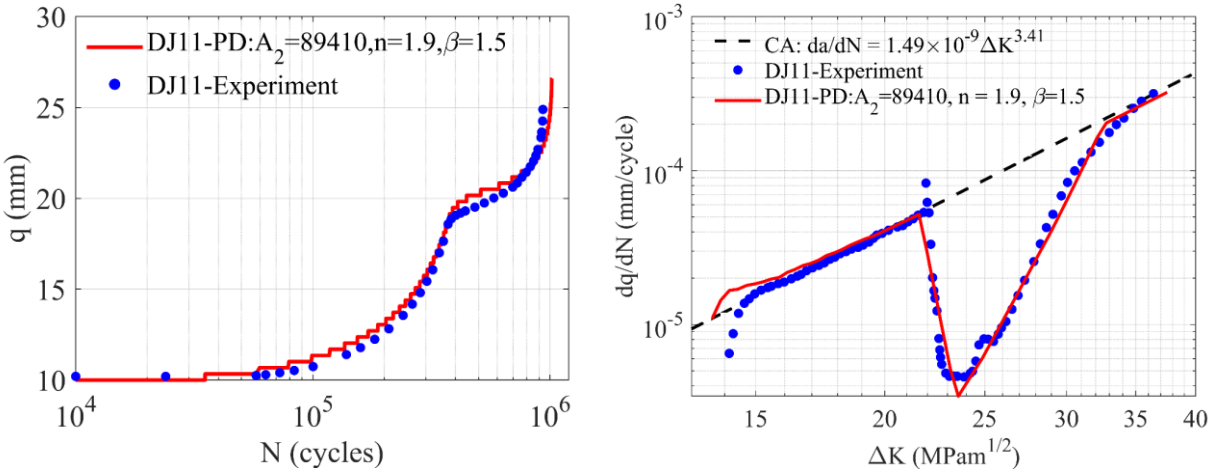

(a) (b)

Fig. 7. Fatigue crack growth on specimen DJ11 (a): $q - N$ curve, (b): $dq/dN - \Delta K$ curve

Fig. 8 and Fig. 9 show the predicted fatigue crack growth for DJ10 and DJ19 specimens, respectively. Here, the DJ10 specimen is subjected to loading with $P_{max} = 5.0$ kN, $R = 0.5$ and $R_{OL} = 1.5$. Meanwhile, the DJ19 specimen is subjected to loading with $P_{max} = 5.0$ kN, $R = 0.5$ and $R_{OL} = 2.0$. The overloads were applied on these specimens when the crack lengths were at $q_{OL} \approx 20.8$ mm. As shown in Fig. 8(b) and Fig. 9(b), the applied overloads caused slight decreases in the fatigue crack growth rates for both specimens. Therefore, after the occurrence of overloads, only slight changes in the crack growth $q - N$ curves are observed for both specimens as shown in Fig. 8(a) and Fig. 9(a). As shown in the figures, PD and experimental results have a good agreement.

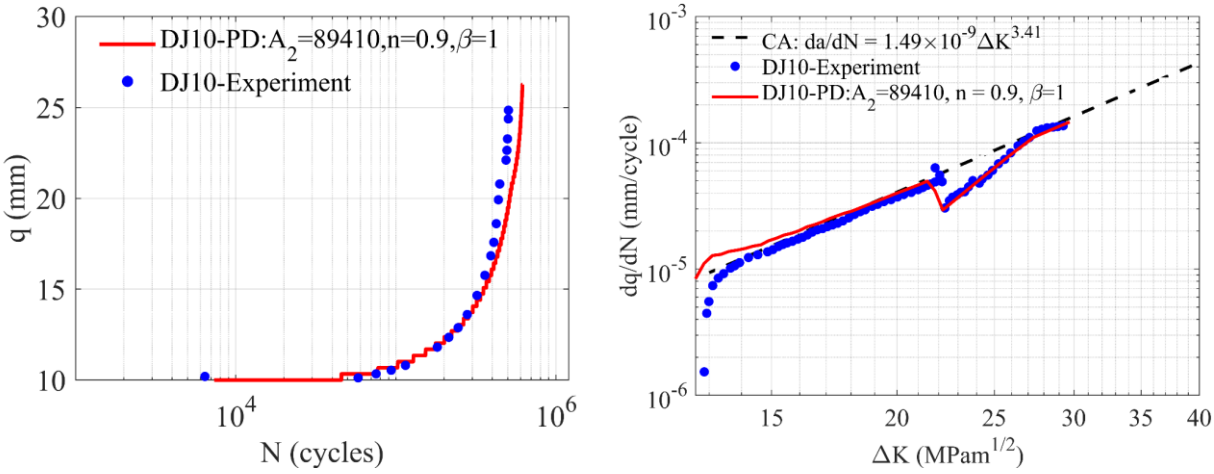

(a) (b)

Fig. 8. Fatigue crack growth on specimen DJ10 (a): $q - N$ curve, (b): $dq/dN - \Delta K$ curve

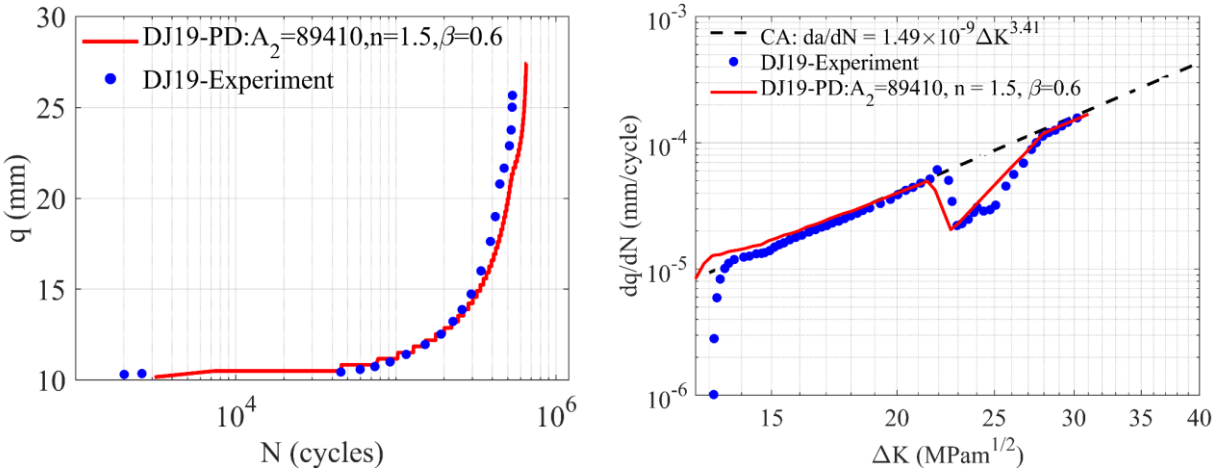

(a) (b)

Fig. 9. Fatigue crack growth on specimen DJ19 (a): $q - N$ curve, (b): $dq/dN - \Delta K$ curve

Fig. 10 shows the predicted fatigue crack growth for DJ08 specimen with $P_{max} = 3.0$ kN, $R = 0.2, R_{OL} = 2.0$. The overload of $P_{OL} = 6.0$ kN was applied when the crack length was approximately $q_{OL} \approx 21.6$ mm. After the occurrence of the overload, the fatigue crack growth rate dq/dN droped significantly to around 5×10^{-6} mm/cycle as shown in Fig. 10(b). As the result, the $q - N$ curve for specimen DJ08 was changed significantly due to the reduction of fatigue crack growth rate as shown in Fig. 10(a). As can be observed from Fig. 10, the fatigue crack growth results predicted by using the PD model have good agreement with the experimental results.

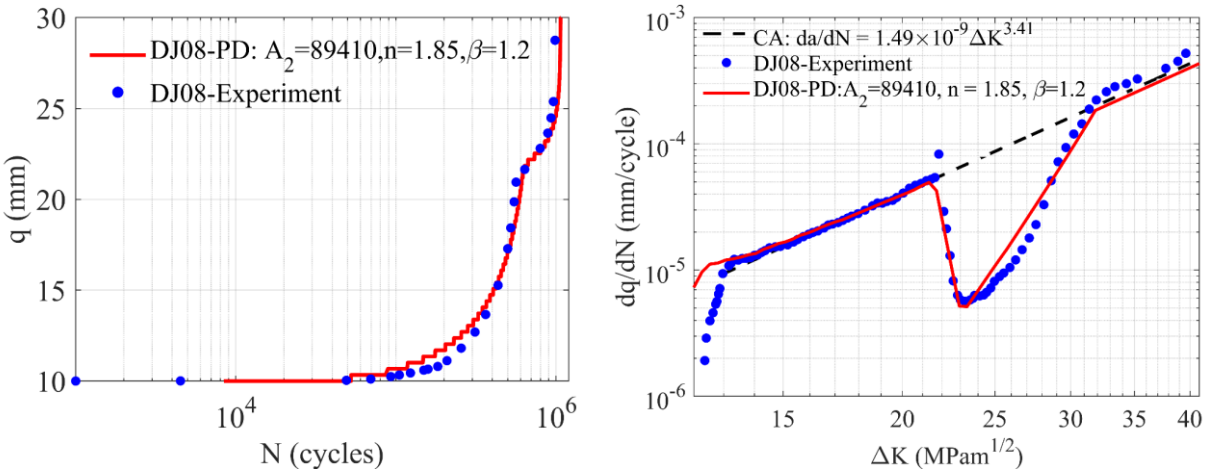

(a) (b)

Fig. 10. Fatigue crack growth on specimen DJ08 (a): $q - N$ curve, (b): $dq/dN - \Delta K$ curve

Fig. 11 shows the PD prediction for fatigue crack growth $q - N$ curves of all investigated specimens subjected to constant amplitude loading with and without the occurrences of overloads. It is observed from the figures that the overloads can significantly extend the fatigue life of the investigated specimens. Specifically, as shown in Fig. 11(a, b), by applying the single overloads with the overload ratio of $R_{OL} = 1.5$ and 2.0 on the constant amplitude loading of $P_{max} = 3.0$ kN, $R = 0.1$, the fatigue life of specimens DJ02 and DJ11 were increased by 48700 and 555670

cycles, respectively. As shown in Fig. 11(c, d), by applying the single overloads with $R_{OL} = 1.5$ and 2.0 on the constant amplitude loading of $P_{max} = 5.0$ kN, $R = 0.5$, the fatigue life of specimens DJ10 and DJ19 were increased by 27380 and 56510 cycles, respectively. As shown in Fig. 11(e), the fatigue life of specimen DJ08 was also increased by 370472 cycles by applying an overload with $R_{OL} = 2.0$ on the constant amplitude loading of $P_{max} = 3.0$ kN, $R = 0.2$.

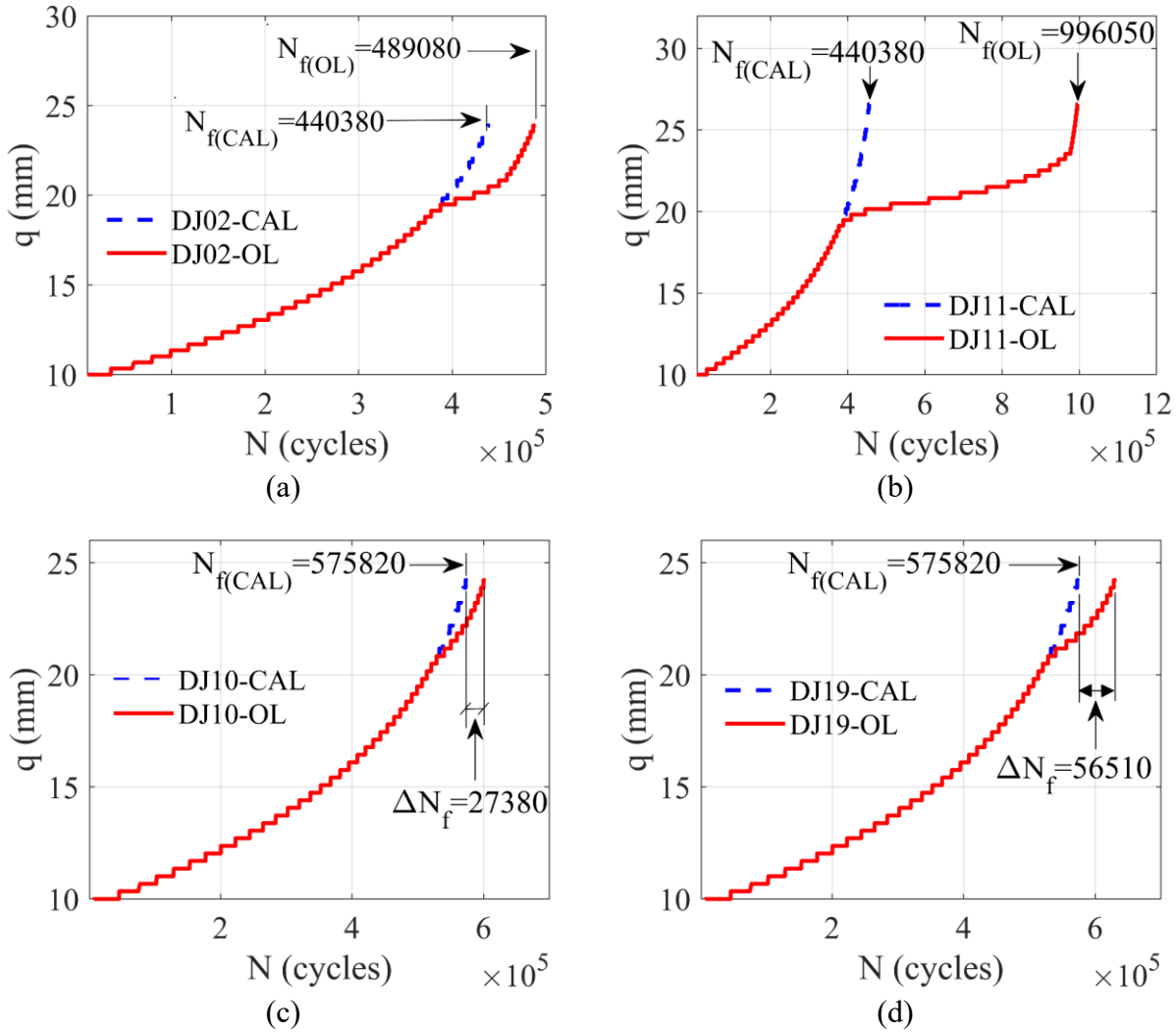

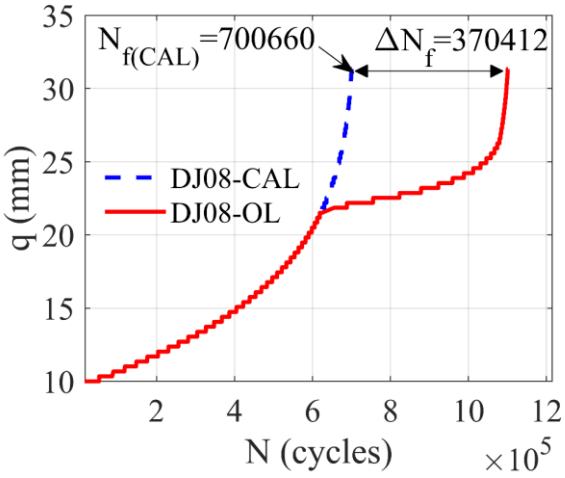

(e)

Fig. 11. PD prediction for fatigue crack growth $q - N$ curves for specimens (a): DJ02, (b): DJ11, (c): DJ10, (d): DJ19, (e): DJ08 when they are subjected to constant amplitude loading with and without the occurrences of overloads.

To further analyze the effects of the overloads on fatigue crack growth, the extensions of fatigue life due to overloads, ΔN_f, for different specimens are presented in Table 3. Here, the extensions of fatigue life due to overloads, ΔN_f is calculated as

$$\Delta N_f = N_{f(\mathrm{OL})} - N_{f(\mathrm{CAL})} \tag{29}$$

where $N_{f(\mathrm{CAL})}$ represents the fatigue life of the specimen when it is subjected to constant amplitude loading. Meanwhile, $N_{f(\mathrm{OL})}$ represents the fatigue life of the specimen when it is subjected to constant amplitude loading with an overload.

It can be observed from Table 3 that the amount of fatigue life extension, ΔN_f is sensitive with overload ratio R_{OL} and loading ratio R. To analyze the relationship between ΔN_f and R_{OL}, groups of specimens with the same constant amplitude loading such as DJ02 and DJ11 with $P_{max} = 3.0$ kN, $R = 0.1$; DJ10 and DJ19 with $P_{max} = 5.0$ kN, $R = 0.5$ are considered. As can be observed from Table 3, by applying the overload with $R_{OL} = 1.5$, the fatigue life of specimen DJ02 was increased by 11.05%. Meanwhile, by applying the overload with $R_{OL} = 2.0$, the fatigue life of specimen DJ11 was increased by 126.18%. Similarly, by applying the overloads with $R_{OL} = 1.5$ and 2.0, the fatigue life of specimen DJ10 and DJ19 were increased by 4.76% and 9.81%, respectively. Therefore, it can be concluded that the amount of fatigue life extension, ΔN_f is increased as the overload ratio increases.

On the other hand, to analyze the relationship between ΔN_f and R, groups of specimens with the same overload ratio such as DJ02 and DJ10 with $R_{OL} = 1.5$; DJ11, DJ19, and DJ08 with $R_{OL} = 2.0$ are considered. As presented in Table 3, the fatigue life of specimen DJ10 with $R = 0.5, R_{OL} = 1.5$ was increased by 4.76%. Meanwhile, the fatigue life of specimen DJ02 with $R = 0.1, R_{OL} = 1.5$ was increased by 11.05%. Moreover, the fatigue lives of specimens DJ11, DJ08 and DJ19 with $R = 0.1, 0.2$, and 0.5 were increased by 126.18%, 52.87%, and 9.81%, respectively. Therefore, it

can be concluded that the amount of the fatigue life extension is decreased as the loading ratio R increases.

Table 3. Predicted extensions of fatigue life for specimens due to single overloads

Specimen	P_{max} (kN)	R	P_{OL} (kN)	R_{OL}	ΔK_{OL} $\left(\text{MPa}\sqrt{\text{m}}\right)$	$N_{f(\text{CAL})}$ (cycles)	ΔN_f (cycles)	$\frac{\Delta N_f}{\Delta N_{f(\text{CAL})}} \times 100\%$
DJ02	3.0	0.1	4.5	1.5	21.80	440380	48700	11.05%
DJ11	3.0	0.1	6.0	2.0	21.80	440380	555670	126.18%
DJ10	5.0	0.5	7.5	1.5	21.80	575820	27380	4.76%
DJ19	5.0	0.5	10.0	2.0	21.80	575820	56510	9.81%
DJ08	3.0	0.2	6.0	2.0	21.80	700660	370412	52.87%

5.3. Single underload and overload-underload combinations

In this section, the proposed PD model is used to predict fatigue crack growth for different loading scenarios which are combinations of underloads and overloads as presented in Table 4 [47]. As shown in Table 4, specimen DJ07 is subjected to a constant amplitude loading with $P_{max} = 4.0$ kN and $R = 0.1$. An underload of $P_{UL} = -6.0$ kN is applied on the specimen when the stress intensity factor is 23.22 MPa$\sqrt{\text{m}}$. Afterward, when the stress intensity factor on the specimen is 30.36 MPa$\sqrt{\text{m}}$, an overload of $P_{OL} = 6.0$ kN followed by an underload of $P_{UL} = -6.0$ kN are applied on the specimen. On the other hand, specimen DJ12 is subjected to a constant amplitude loading with $P_{max} = 3.0$ kN and $R = 0.1$. An overload of $P_{OL} = 6.0$ kN followed by an underload of $P_{UL} = -6.0$ kN are applied twice on the specimen when the stress intensity factors are 17.07 MPa$\sqrt{\text{m}}$ and 22.15 MPa$\sqrt{\text{m}}$, respectively.

Table 4. Constant amplitude loading with underload and overload-underload combinations

Specimen	P_{max} (kN)	R	P_{OL} (kN)	R_{OL}	P_{UL} (kN)	ΔK_{UL} $\left(\text{MPa}\sqrt{\text{m}}\right)$	$\Delta K_{OL/UL}$ $\left(\text{MPa}\sqrt{\text{m}}\right)$	$\Delta K_{UL/OL}$ $\left(\text{MPa}\sqrt{\text{m}}\right)$
DJ07	4.0	0.1	6.0	1.5	-6.0	23.22	30.36	--
DJ12	3.0	0.1	6.0	2.0	-6.0	--	17.07	22.15

By using the calibration procedure as presented in Appendices B and C, the crack length at the end of the delay retardation process, q_d and the best-fit coefficients (β, n) for modified Wheeler models for specimens DJ07 and DJ12 are obtained as presented in Table 5. In Table 5, the coefficients (β_{UL}, n_{UL}) are used to calculate the retardation factor due to single underloads as given in Eq. (22) in Section 3.3. Meanwhile, the parameters $(q_d, \phi_{Rd}, \beta_{OL}, n_{OL})$ are used to calculate the retardation factor due to overloads given in Eq. (25) in Section 3.4.

Table 5. Best-fit coefficients (β, n) and the predicted q_d for DJ07 and DJ12

Specimen	Single underload	The first overload/underload	The second overload/underload
DJ07	Parameters for underload: $q_{UL} = 15.2$ mm; $\beta_{UL} = 0.52$; $n_{UL} = 1.25$	Parameters for overload: $q_{OL} = 20.52$ mm; $q_d = 22.4$ mm; $\phi_{Rd} = 0.716$; $\beta_{OL} = 1.2$; $n_{OL} = 0.6$ Parameters for underload: $\beta_{UL} = 0.52$; $n_{UL} = 1.25$	--
DJ12	--	Parameters for overload: $q_{OL} = 14.51$ mm; $q_d = 15.50$ mm; $\phi_{Rd} = 0.3512$; $\beta_{OL} = 1.7$; $n_{OL} = 0.5$ Parameters for underload: $\beta_{UL} = 0.52$; $n_{UL} = 0.66$	Parameters for overload: $q_{OL} = 19.64$ mm; $q_d = 21.30$ mm; $\phi_{Rd} = 0.0538$; $\beta_{OL} = 1.4$; $n_{OL} = 1.9$ Parameters for underload: $\beta_{UL} = 0.52$; $n_{UL} = 0.66$

By using the calibrated parameters presented in Table 5, the fatigue crack growth on specimens DJ07 and DJ12 are predicted by using the proposed PD model as shown in Fig. 12 and Fig. 13. Fig. 12 shows the predicted fatigue crack growth for specimen DJ07. As shown in Fig. 12(a), when the crack length on the specimen is $q_f = 26.26$ mm, the fatigue life obtained by experiment is $N_{f(\text{experiment})} = 1.80335 \times 10^5$ [47]. Meanwhile, the fatigue life predicted by using PD model is $N_{f(\text{PD})} = 1.728 \times 10^5$, which is 4.18% different than the experimental result. As shown in Fig. 12(b), the predicted $dq/dN - \Delta K$ curve for specimen DJ07 also agrees well with the experimental data.

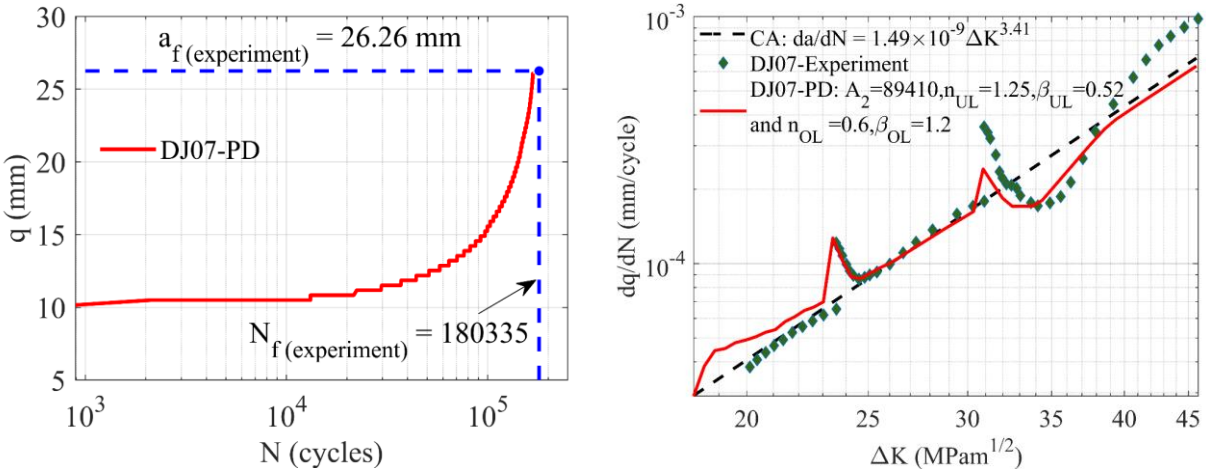

(a) (b)

Fig. 12. Fatigue crack growth on specimen DJ07 (a): $q - N$ curve, (b): $dq/dN - \Delta K$ curve

Fig. 13 shows the predicted fatigue crack growth for the specimen DJ12. As shown in Fig. 13(a), when the crack length on the specimen is $q_f = 27.554$ mm, fatigue life obtained by experiment is $N_{f(\text{experiment})} = 1.026456 \times 10^6$ [47]. Meanwhile, the fatigue life predicted by using the PD model is $N_{f(\text{PD})} = 9.982 \times 10^5$, which is 2.75% different than the experimental result.

As shown in Fig. 13(b), the predicted $dq/dN - \Delta K$ curve agrees very well with the experimental results [47]. Moreover, it can be observed from Fig. 13(b) that the second overload/underload was applied when the fatigue crack growth rate dq/dN on specimen DJ12 has not fully returned to the stable crack growth rate of the constant amplitude loading. Therefore, the second overload/underload combination created a significant drop for the fatigue crack growth rate dq/dN as shown in Fig. 13(b). As a result, a significant extension on the fatigue life of the specimen is observed as shown in Fig. 13(a).

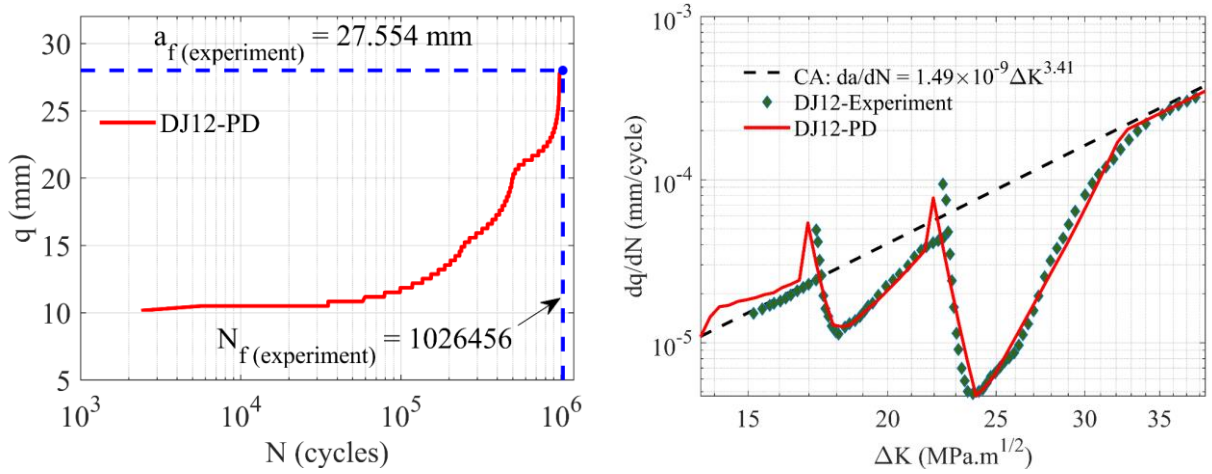

(a) (b)

Fig. 13. Fatigue crack growth on specimen DJ12 (a): $q - N$ curve, (b): $dq/dN - \Delta K$ curve

To further analyze the effects of variable amplitude loading on the fatigue crack growth, the predicted $q - N$ curve for specimen DJ07 subjected to variable amplitude loading is compared with the predicted $q - N$ curve when it is subjected to constant amplitude loading with $P_{max} = 4.0$ kN, $R = 0.1$ as shown in Fig. 14(a). In this figure, the $q - N$ curve for specimen DJ07 subjected to variable amplitude loading is shown in red. Meanwhile, the $q - N$ curve for specimen DJ07 subjected to constant amplitude loading is shown in blue. It is observed from Fig. 14(a) that when the crack length was around 16 mm, the underload was applied, and it created a slight increase in the fatigue crack growth rate afterwards. Therefore, at the same value of N, the predicted crack length for specimen DJ07 with underload is slightly higher than the predicted crack length in the constant amplitude loading case. Later, the applied overload/underload created a slight decrease in the crack growth rate. Therefore, the predicted $q - N$ curve for specimen DJ07 subjected to variable amplitude loading becomes very close to the $q - N$ curve in the constant amplitude loading.

Similarly, the predicted $q - N$ curve for specimen DJ12 subjected to variable amplitude loading is compared with the predicted $q - N$ curve when it is subjected to constant amplitude loading with $P_{max} = 3.0$ kN, $R = 0.1$ as shown in Fig. 14(b). In this figure, the $q - N$ curve for specimen

DJ12 subjected to variable amplitude loading is shown in red. Meanwhile, the $q-N$ curve for specimen DJ12 subjected to constant amplitude loading is shown in blue. As can be observed from this figure, both the applied underload/overload and overload/underload created significant decreases in the fatigue crack growth rate. The predicted fatigue life of specimen DJ12 when it is subjected to variable amplitude loading is 977693 cycles which is equal to 213.56% of the fatigue life of it in the constant amplitude loading case.

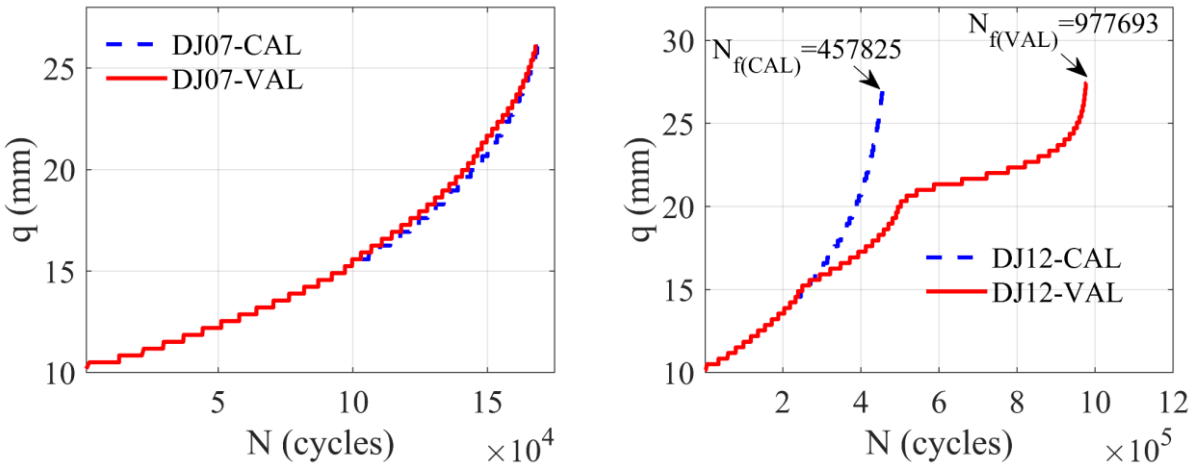

(a) (b)

Fig. 14. PD prediction for fatigue crack growth $q-N$ curves for specimens (a): DJ07, (b): DJ12 when they are subjected to constant amplitude loading with and without the occurrences of overloads and underloads.

6. Conclusion

In this study, a novel PD model for the prediction of fatigue crack growth with the effects of overload and underload is proposed. The modified Wheeler models to consider the effects of single overloads, underloads and overload-underload combinations are proposed and successfully applied to PD fatigue equations. The numerical procedure to predict fatigue cracking by using the proposed PD model is presented.

The capability of the proposed PD model is verified by considering fatigue crack growth on a single edge-notch plate subjected to constant amplitude loading and various loading scenarios with the occurrence of overloads and underloads. The fatigue crack growth $q-N$ and $dq/dN-\Delta K$ curves predicted by the proposed PD model show good agreement with the experimental results.

Moreover, the proposed PD model is further used to predict the extensions of fatigue life, ΔN_f, for all variable amplitude loading cases. From this further prediction, the relationships between the amount of fatigue life extension, ΔN_f, the loading ratio, R, and the overload ratio, R_{OL} are discovered. Specifically, the amount of fatigue life extension, ΔN_f can be increased as the overload ratio, R_{OL} increases and the loading ratio, R decreases.

Acknowledgement

The results were obtained using the ARCHIE-WeSt High-Performance Computer (www.archie-west.ac.uk) based at the University of Strathclyde.

Appendix A. Calibrations for parameters for overloads

As presented in Section 3.2, there are 3 main parameters that need to be calibrated from experimental data, including the crack length at the end of the delay retardation process, q_d and the coefficients (β, n) for the modified Wheeler model. In this section, first, the determination of the crack length at the end of the delay retardation process, q_d is presented in Section A1. Next, two-step calibration process to obtain values for (ϕ_{Rd}, β, n) is presented in Section A2.

A1. Determination of crack length at the end of the delay retardation process, q_d

In this section, the determination of the crack length at the end of the delay retardation process, q_d is presented. As presented in Eq. (20) in Section 3.2, the crack length at the end of the delay retardation process, q_d, is assumed to have the relationship with q_{OL}, r_{OL}, R, and R_{OL} as

$$\frac{q_d - q_{OL}}{r_{OL}} = f(R, R_{OL}) \tag{A1a}$$

or

$$q_d = q_{OL} + r_{OL} f(R, R_{OL}) \tag{A1b}$$

where R_{OL} represents the overloading ratio which can be defined as

$$R_{OL} = P_{OL}/P_{max} \tag{A2}$$

In this study, the relationship given in Eq. (A1) for Q345R steel material used in Section 5 is determined by using linear regression for the experimental data. First, from experimental data for Q345R steel [47], the stress intensity factor corresponding to the end of the delay retardation process, ΔK_d for each case given in Table 1 is determined. ΔK_d is defined as the stress intensity factor corresponding to the lowest point on the $dq/dN - \Delta K$ curve as shown in Fig. 15.

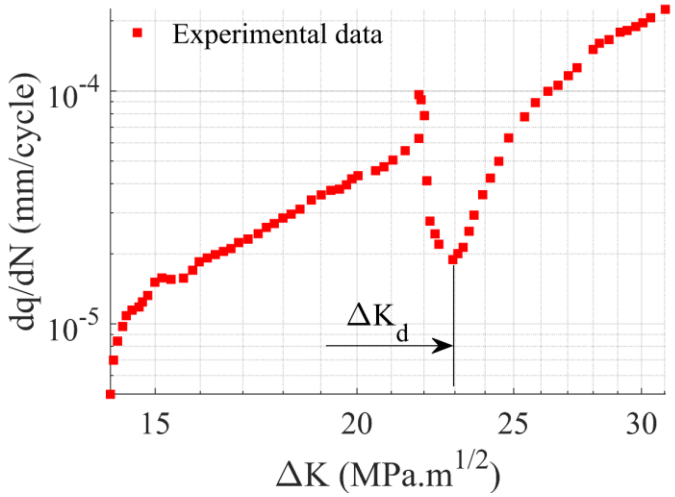

Fig. 15. Determination of the stress intensity factor corresponding to the end of the delay retardation process, ΔK_d

Next, the crack length at the end of the delay retardation process, q_d can be determined as a root of the following equation [50]

$$\Delta K_d = \frac{\Delta P(2+\xi_d)}{h\sqrt{W}(1-\xi_d)^{3/2}}(0.886 + 4.64\xi_d - 13.32\xi_d^2 + 14.72\xi_d^3 - 5.6\xi_d^4) \tag{A3a}$$

with

$$\xi_d = \frac{q_d}{W} \tag{A3b}$$

$$\Delta P = P_{max}(1 - R) \tag{A3c}$$

$$W = 0.0508 \text{ m}, h = 0.0038 \text{ m} \tag{A3d}$$

In this study, to determine q_d from Eq. (A3a), various values of q_d with very small increments are assumed. The corresponding values for the right-hand side of Eq. (A3a) are calculated. Therefore, from the various values of the right-hand side, the closest value with ΔK_d is determined and q_d is found accordingly.

The obtained values for q_d for specimens DJ02, DJ08, DJ10, DJ11 and DJ19 are given in Table 6. It is observed from Table 6 that the term $(q_d - q_{OL})/r_{OL}$ is only sensitive to the loading ratio, R. Therefore, by using linear regression, the following possible relations between $(q_d - q_{OL})/r_{OL}$ and loading ratio R can be proposed as

$$\frac{q_d - q_{OL}}{r_{OL}} = -0.42132R + 0.24132, \text{ with RMS} = 0.02319 \tag{A4a}$$

or

$$\frac{q_d - q_{OL}}{r_{OL}} = -1.37365R + 1.55031R^2 + 0.33434, \text{ with RMS} = 0.01442 \tag{A4b}$$

or

$$\frac{q_d - q_{OL}}{r_{OL}} = -1.22352R + 0.84385R^2 + 0.88308R^3 + 0.32551, \text{ with RMS} = 0.01442 \tag{A4c}$$

Table 6. The crack length at the end of the delay retardation process, q_d for different specimens

Specimen	P_{max} (kN)	R	P_{OL} (kN)	R_{OL}	r_{OL} (m)	q_{OL} (m)	ΔK_d $(\text{MPa}\sqrt{\text{m}})$	q_d (m)	$\frac{(q_d - q_{OL})}{r_{OL}}$
DJ02	3.0	0.1	4.5	1.5	4.1695E-3	1.933E-2	22.822	2.031E-2	2.350E-1
DJ08	3.0	0.2	6.0	2.0	9.7842E-3	2.158E-2	23.253	2.277E-2	1.216E-1
DJ10	5.0	0.5	7.5	1.5	1.4161E-2	2.081E-2	22.378	2.126E-2	3.178E-2
DJ11	3.0	0.1	6.0	2.0	7.6874E-3	1.933E-2	23.732	2.079E-2	1.899E-1
DJ19	5.0	0.5	10.0	2.0	2.5252E-2	2.081E-2	22.847	2.178E-2	3.841E-2

The variations of $(q_d - q_{OL})/r_{OL}$ versus loading ratio R obtained by using Eqs. (A4a-c) are shown in Fig. 16. As can be observed from Fig. 16, the linear relationship given in Eq. (A4a) gives significant root mean square (RMS) error of 0.02319. Meanwhile, both quadratic and cubic polynomial relations give the same value of root mean square with $\text{RMS} = 0.01442$. Moreover, both polynomial relations give similar results of $(q_d - q_{OL})/r_{OL}$ for the loading ratio of $0 \leq R \leq 0.5$. Therefore, in this study, the quadratic relation given in Eq. (A4b) is chosen to simplify the relationship.

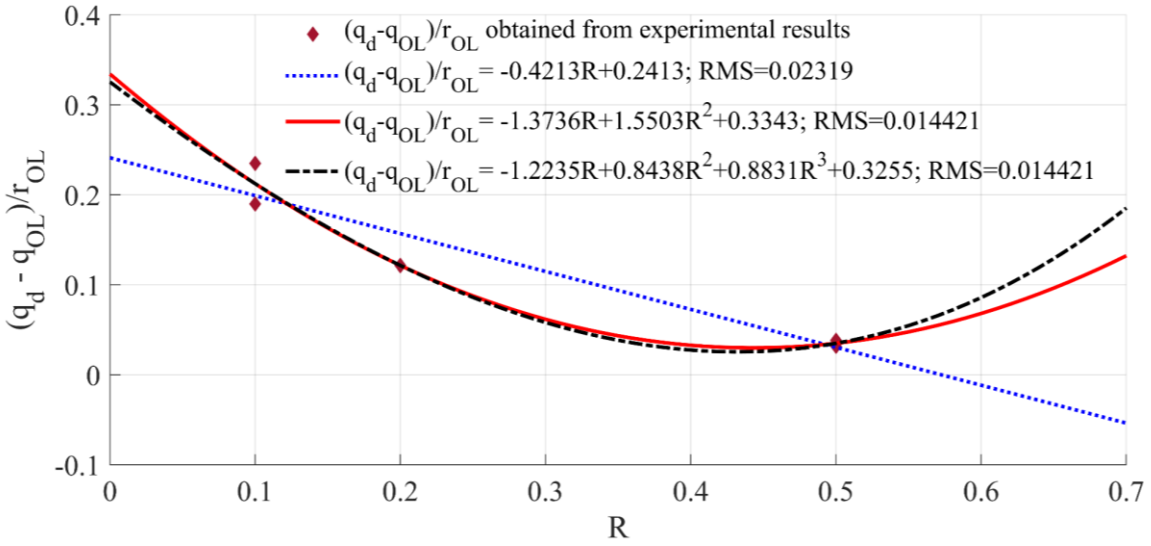

Fig. 16. Variations of $(q_d - q_{OL})/r_{OL}$ versus loading ratio R

By using the quadratic polynomial given in Eq. (A4b), the predicted values for $(q_d - q_{OL})/r_{OL}$ and ΔK_d and the relative errors between these predicted values and those obtained from experimental data are presented in Table 7. In this table, $((q_d - q_{OL})/r_{OL})^*$ and ΔK_d^* represent the predicted values for $(q_d - q_{OL})/r_{OL}$ and ΔK_d, respectively. As can be seen from Table 7, the relative errors of the predicted $(q_d - q_{OL})/r_{OL}$ are smaller than 12%, meanwhile, the relative errors of the predicted ΔK_d are less than 1%.

Finally, by using the quadratic polynomial given in Eq. (A4b), the crack length at the end of the delay retardation process, q_d can be predicted as

$$q_d = q_{OL} + r_{OL}(-1.37365R + 1.55031R^2 + 0.33434) \quad \text{(A5)}$$

By using Eq. (A5), the predicted value for the crack length at the end of the delay retardation process q_d^* for different overloading cases investigated in Section 5.2 are presented in Table 7.

Table 7. Specimens for Q345R steel and the predicted values for $(q_d - q_{OL})/r_{OL}$ and ΔK_d

Specimen	$\frac{q_d - q_{OL}}{r_{OL}}$	$\left(\frac{q_d - q_{OL}}{r_{OL}}\right)^*$	%Error of $\left(\frac{q_d - q_{OL}}{r_{OL}}\right)$	ΔK_d $(\text{MPa}\sqrt{\text{m}})$	ΔK_d^* $(\text{MPa}\sqrt{\text{m}})$	%Error of ΔK_d	q_d^* (m)
DJ02	2.350E-01	2.125E-01	-9.60%	22.934	22.815	-0.52%	0.0202
DJ08	1.216E-01	1.216E-01	0.00%	23.253	23.253	0.00%	0.0228
DJ10	3.178E-02	3.509E-02	10.44%	22.322	22.378	0.25%	0.0213
DJ11	1.899E-01	2.125E-01	11.88%	23.517	23.732	0.91%	0.0210
DJ19	3.841E-02	3.509E-02	-8.64%	22.950	22.847	-0.45%	0.0217

A2. Calibrations for parameters (β, n) for overloads

In this section, two-step calibration process for parameters β, n and ϕ_{Rd} used in the modified Wheeler model for overloads investigated in Sections 5.2 is presented. In the first step, by ignoring the delay retardation process, the calculation of ϕ_R given in Eq. (16) is reduced to a simpler formulation as

$$\phi_R = \begin{cases} \left[\frac{r_i}{q_{OL}+\beta r_{OL}-q_i}\right]^n & \text{if} \quad q_{OL} \le q_i < q_{OL} + \beta r_{OL} - r_i \\ 1 & \text{otherwise} \end{cases} \tag{A6}$$

In Eq. (A6), the plastic zone size due to the overload, r_{OL}, is calculated by using Eq. (19a) in which the plastic zone size factor, α_{OL}, is calculated by using Eq. (19c).

By assuming the crack length q_i varying from q_n to q_f, the corresponding value of plastic zone size due to constant amplitude loading is calculated by using Eq. (19b) and Eq. (19d). Here, q_n is the initial crack length and q_f is the final crack length as provided by experimental data.

Next, various values for β and n with very small increments are assumed. For each pair of values of β and n, the corresponding values for ϕ_R are calculated by using Eq. (A6) and the $(dq/dN)_{VAL} - \Delta K$ curve is obtained by using Eq. (14). Among the obtained $(dq/dN)_{VAL} - \Delta K$ curves, the best-fit $(dq/dN)_{VAL} - \Delta K$ curve is determined. Therefore, the best-fit values for β and n are determined.

To visualize the calibration process, the best-fit results for calibration of specimen DJ02 are shown in Fig. 17. As shown in Fig. 17(a), the best-fit $dq/dN - \Delta K$ curve is shown in blue which corresponds to $\beta = 1.55$ and $n = 1.20$.

In the second step, the delay retardation process is considered. Specifically, the predicted value for q_d as presented in Appendix A1 is used to calculated ΔK_d by using Eq. (A3). Here, q_d is the crack length at the end of the retardation process, and ΔK_d is the stress intensity factor range corresponding to crack length q_d.

By using the obtained value for ΔK_d, point B in the $dq/dN - \Delta K$ curve as shown in Fig. 17(b) is determined. Therefore, the value of ϕ_{Rd}, which is the value of ϕ_R at the end of the delay retardation process, is calculated as

$$\phi_{Rd} = \left[\frac{r_d}{q_{OL}+\beta r_{OL}-q_d}\right]^n \tag{A7}$$

where β and n are obtained from the first calibration step, and r_d is the plastic zone size when the crack length is equal to q_d. This parameter can be calculated by using Eq. (19b) and Eq. (19d) as

$$r_d = \alpha_d \left(\frac{K_d}{\sigma_y}\right)^2 \tag{A8a}$$

with

$$\alpha_d = 0.35 - \frac{0.29}{1+\left[1.08K_d^2/(h\sigma_y^2)\right]^{2.15}} \tag{A8b}$$

and

$$K_d = \Delta K_d/(1-R) \quad \text{(A8c)}$$

Finally, after obtaining values for parameters q_d, β, n and ϕ_{Rd}, the coefficient ϕ_R for the modified Wheeler model for overloads is calculated by using Eq. (16).

Fig. 17(b) shows the finally calibrated $dq/dN - \Delta K$ curve for specimen DJ02. For this specimen, the value of q_d, β, n and ϕ_{Rd} are $q_d = 0.0202$ m, $\beta = 1.55$, $n = 1.20$ and $\phi_{Rd} = 0.2601$, respectively. By using abovementioned two-step calibration process for all specimens, the parameters q_d, β, n, ϕ_{Rd} for all investigated overloads are obtained as presented in Table 2.

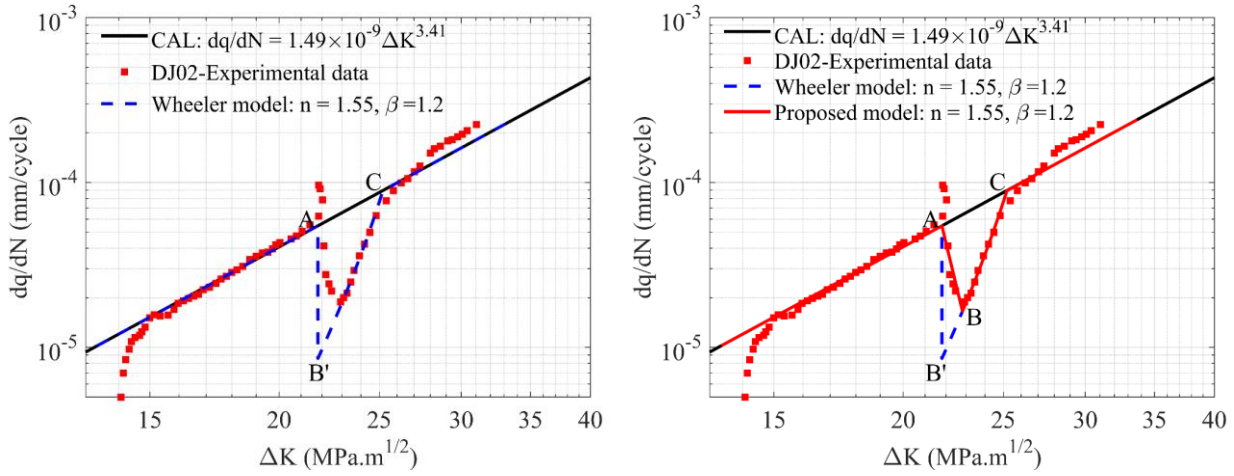

Fig. 17. Two-step calibration process for the proposed modified Wheeler model (a) step 1: finding best-fit values for (β, n) by disregarding the delay retardation process, (b) step 2: the value of q_d is predicted by solving Eq. (A3a) and the value of ϕ_{Rd} is determined by using Eq. (A2). Path $AB'B$ in the Wheeler model is replaced by path AB in the proposed model.

In summary, the two-step calibration process for overloads can be conducted by using the following procedure:

Step 1: Calibrate (β, n) by disregarding the delay retardation process.

- Step 1.1: Determine the crack length at which the overload is applied, q_{OL} by solving the following equation [50]

$$\Delta K_{OL} = \frac{\Delta P(2+\xi_{OL})}{h\sqrt{W}(1-\xi_{OL})^{3/2}}(0.886 + 4.64\xi_{OL} - 13.32\xi_{OL}^2 + 14.72\xi_{OL}^3 - 5.6\xi_{OL}^4) \quad \text{(A9a)}$$

with

$$\xi_{OL} = \frac{q_{OL}}{W} \quad \text{(A9b)}$$

$$\Delta P = P_{max}(1-R) \quad \text{(A9c)}$$

$$W = 0.0508 \text{ m}, h = 0.0038 \text{ m} \quad \text{(A9d)}$$

- Step 1.2: With the value for q_{OL} obtained from step 1.1, the plastic zone size due to the overload is estimated by using Eq. (19a) and Eq. (19c).

- Step 1.3: Assuming various values for crack length, q_i

$$q_i = q_n,\ q_n + \Delta q,\ q_n + 2\Delta q,\ \dots,\ q_f \quad \text{(A9)}$$

where q_n is the initial crack length and q_f is the final crack length as provided by experimental data, Δq is a small increment of crack length.

- Step 1.4: Calculate plastic zone size due to constant amplitude loading, r_i by using Eq. (19b) and Eq. (19d).

- Step 1.5: Assume different values for β and n in a range between 0 and 3

$$\beta = 0.1,\ 0.2,\ 0.3,\ \dots,\ 3 \quad \text{(A10a)}$$

$$n = 0.01,\ 0.02,\ 0.03,\ \dots,\ 3 \quad \text{(A10b)}$$

- Step 1.6: For each pair values of β and n, calculate ϕ_R by using Eq. (A6). In Eq. (A6), the values of q_i are obtained in step 1.1 and the plastic zone size r_i is obtained from step 1.2. Therefore, for each pair values of β and n, the obtained values for ϕ_R will vary as a function of crack length q_i.

- Step 1.7: The stress intensity factor range, ΔK_i, corresponding to the crack length q_i is calculated as [50]

$$\Delta K_i = \frac{\Delta P(2+\xi_d)}{h\sqrt{W}(1-\xi_i)^{3/2}}(0.886 + 4.64\xi_i - 13.32\xi_i^2 + 14.72\xi_i^3 - 5.6\xi_i^4) \quad \text{(A11a)}$$

with

$$\xi_i = \frac{q_i}{W} \quad \text{(A11b)}$$

$$\Delta P = P_{max}(1 - R) \quad \text{(A11c)}$$

$$W = 0.0508\ \text{m}, h = 0.0038\ \text{m} \quad \text{(A11d)}$$

- Step 1.8: By using Eq. (14), $(dq/dN)_{VAL} - \Delta K$ curve for current value of β and n is obtained.

- Step 1.9: Repeating steps 1.6, 1.7, and 1.8 for all possible pair values of β and n, all possible $(dq/dN)_{VAL} - \Delta K$ curves are obtained.

- Step 1.10: By comparing all possible $(dq/dN)_{VAL} - \Delta K$ curves obtained in step 1.9 with the experimental data, the best-fit $(dq/dN)_{VAL} - \Delta K$ curve is determined. Therefore, the best-fit values for β and n are also determined accordingly.

Step 2: Calculate of the crack length at the end of the delay retardation process, q_d and ϕ_{Rd} by considering the delay retardation process.

- Step 2.1: Calculate the crack length at the end of the delay retardation process, q_d by using Eq. (A5).

- Step 2.2: Calculate the plastic zone size corresponding to the crack length q_d by using Eq. (A8).

- Step 2.2: Calculate ϕ_{Rd} by using Eq. (A7).

Step 3: Finally, calculate the retardation factor ϕ_R for the overload by using Eq. (16).

Appendix B. Calibrations for parameters for underloads

In the example investigated in Section 5.3, specimen DJ07 is subjected to a single underload with $P_{UL} = -6.0$ kN. The coefficient ϕ_R for the underloading effects is calculated by using Eq. (22) as

$$\phi_R = \begin{cases} \left[\frac{\beta\, r_{UL}}{q_i + r_i - q_{UL}}\right]^n & \text{if} \quad q_{UL} \le q_i \le q_{UL} + \beta r_{UL} - r_i \\ 1 & \text{if} \quad q_i + r_i > q_{UL} + \beta r_{UL} \end{cases} \tag{B1a}$$

with

$$r_{UL} = \alpha_{UL}\left(\frac{\Delta K_{UL}}{\sigma_Y}\right)^2 = \alpha_{UL}\left(\frac{K_{min,CA} - K_{\min,UL}}{\sigma_Y}\right)^2 \tag{B1b}$$

and

$$\alpha_{UL} = 0.35 - \frac{0.29}{1 + \left[\frac{1.08\left(K_{min,CA} - K_{\min,UL}\right)^2}{h\sigma_y^2}\right]^{2.15}} \tag{B1c}$$

The calibration for parameters β and n for a single underload is similar to the first step calibration for a single overload as presented in Appendix A2. The calibration procedure for underloads can be summarized as follows:

Step 1: Determine the crack length at which the underload is applied, q_{UL} by solving the following equation [50]

$$\Delta K_{UL} = \frac{\Delta P(2+\xi_{UL})}{h\sqrt{W}(1-\xi_{UL})^{3/2}}(0.886 + 4.64\xi_{UL} - 13.32\xi_{UL}^2 + 14.72\xi_{UL}^3 - 5.6\xi_{UL}^4) \tag{B2a}$$

with

$$\xi_{UL} = \frac{q_{UL}}{W} \tag{B2b}$$

$$\Delta P = P_{max}(1 - R) \tag{B2c}$$

$$W = 0.0508 \text{ m}, h = 0.0038 \text{ m} \tag{B2d}$$

Step 2: Determine the term, $\Delta K_{min,UL} = K_{min,CAL} - K_{\min,UL}$ given in Eq. (23b) as [50]

$$\Delta K_{min,UL} = \frac{(P_{min} - P_{UL})(2+\xi_{UL})}{h\sqrt{W}(1-\xi_{UL})^{3/2}}(0.886 + 4.64\xi_{UL} - 13.32\xi_{UL}^2 + 14.72\xi_{UL}^3 - 5.6\xi_{UL}^4) \tag{B3a}$$

where h and W are given in Eq. (B2d), $\xi_{UL} = q_{UL}/W$ is obtained from step 1.

Step 3: With the value for q_{UL} obtained in step 1 and $\Delta K_{min,UL}$ obtained in step 2, the plastic zone size due to the underload is estimated by using Eq. (23a) and Eq. (23c).

Step 4: Assume various values for crack length, q_i

$$q_i = q_n,\ q_n + \Delta q,\ q_n + 2\Delta q,\ \ldots,\ q_f \tag{B4}$$

where q_n is the initial crack length and q_f is the final crack length as provided by experimental data, Δq is a small increment of crack length.

Step 5: Calculate plastic zone size due to constant amplitude loading, r_i by using Eq. (19b) and Eq. (19d).

Step 6: Assume different values for β and n

$$\beta = 0.1,\ 0.2,\ 0.3,\ \ldots, 3 \tag{B5a}$$

$$n = 0.01,\ 0.02,\ 0.03,\ \ldots, 3 \tag{B5b}$$

Step 7: For each pair values of β and n, calculate ϕ_R by using Eq. (B1). In Eq. (B1), the values of q_i are obtained in step 4 and the plastic zone size r_i is obtained from step 5. Therefore, for each pair values of β and n, the obtained values for ϕ_R will vary as a function of crack length q_i.

Step 8: The stress intensity factor range, ΔK_i, corresponding to the crack length q_i is calculated as [50]

$$\Delta K_i = \frac{\Delta P(2+\xi_d)}{h\sqrt{W}(1-\xi_i)^{3/2}}(0.886 + 4.64\xi_i - 13.32\xi_i^2 + 14.72\xi_i^3 - 5.6\xi_i^4) \tag{B6a}$$

with

$$\xi_i = \frac{q_i}{W} \tag{B6b}$$

$$\Delta P = P_{max}(1 - R) \tag{B6c}$$

$$W = 0.0508\ \text{m}, h = 0.0038\ \text{m} \tag{B6d}$$

Step 9: By using Eq. (14), $(dq/dN)_{VAL} - \Delta K$ curve for current value of β and n is obtained.

Step 10: Repeating steps 7, 8, and 9 for all possible pair values of β and n, all possible $(dq/dN)_{VAL} - \Delta K$ curves are obtained.

Step 11: By comparing all possible $(dq/dN)_{VAL} - \Delta K$ curves obtained in step 10 with the experimental data, the best-fit $(dq/dN)_{VAL} - \Delta K$ curve is determined. Therefore, the best-fit values for β and n for the underload are also determined accordingly.

Appendix C. Calibrations for parameters for underload-overload combinations

In Section 5.3, specimen DJ07 is subjected to a single overload of $P_{OL} = 6.0$ kN followed by a single underload of $P_{UL} = -6.0$ kN when the stress intensity factor on the specimen is 30.36 MPa$\sqrt{\text{m}}$. Meanwhile, specimen DJ12 is subjected to single overload of $P_{OL} = 6.0$ kN followed by a single underload of $P_{UL} = -6.0$ kN when the stress intensity factors are 17.07 MPa$\sqrt{\text{m}}$ and 22.15 MPa$\sqrt{\text{m}}$, respectively. Details for these loading conditions are presented in Table 4.

To consider the effects of overload/underload, the retardation coefficient ϕ_R is calculated by using Eq. (24) in Section 3.4 as

$$\phi_R = \phi_{R,OL} \times \phi_{R,UL} \tag{C1}$$

The calibration process for parameters β_{UL}, n_{UL} for the calculation of $\phi_{R,UL}$ follows the same procedure presented in Appendix B. The calibration process for parameters $q_d, \phi_{Rd}, \beta_{OL}, n_{OL}$ for

the calculation of $\phi_{R,OL}$ follows the same procedure presented in Appendix A2 except for step 3. Specifically, Eq. (25) is used to calculate ϕ_R in step 3 instead of Eq. (16).

References

[1] O.E. Wheeler, Spectrum loading and crack growth, (1972).
[2] B. Yuen, F. Taheri, Proposed modifications to the Wheeler retardation model for multiple overloading fatigue life prediction, International journal of fatigue, 28 (2006) 1803-1819.
[3] F. Taheri, D. Trask, N. Pegg, Experimental and analytical investigation of fatigue characteristics of 350WT steel under constant and variable amplitude loadings, Marine Structures, 16 (2003) 69-91.
[4] X. Huang, M. Torgeir, W. Cui, An engineering model of fatigue crack growth under variable amplitude loading, International Journal of Fatigue, 30 (2008) 2-10.
[5] P.A. Rushton, F. Taheri, Prediction of crack growth in 350WT steel subjected to constant amplitude with over-and under-loads using a modified wheeler approach, Marine structures, 16 (2003) 517-539.
[6] M.V.S. Pereira, F.A.I. Darwish, A.F. Camarão, S.H. Motta, On the prediction of fatigue crack retardation using Wheeler and Willenborg models, Materials Research, 10 (2007) 101-107.
[7] M. Mehrzadi, F. Taheri, A material sensitive modified wheeler model for predicting the retardation in fatigue response of AM60B due to an overload, International journal of fatigue, 55 (2013) 220-229.
[8] J. Barsom, Fatigue crack growth under variable-amplitude loading in various bridge steels, in: Fatigue Crack Growth under Spectrum Loads, ASTM International, 1976.
[9] A. De Koning, A simple crack closure model for prediction of fatigue crack growth rates under variable-amplitude loading, in: Fracture mechanics, ASTM International, 1981.
[10] Y. Kondo, Fatigue under variable amplitude loading, (2003).
[11] M. Sander, H. Richard, Fatigue crack growth under variable amplitude loading Part II: analytical and numerical investigations, Fatigue & Fracture of Engineering Materials & Structures, 29 (2006) 303-319.
[12] B. Ziegler, Y. Yamada, J. Newman Jr, Application of a strip-yield model to predict crack growth under variable-amplitude and spectrum loading–Part 2: Middle-crack-tension specimens, Engineering fracture mechanics, 78 (2011) 2609-2619.
[13] F. Chen, F. Wang, W. Cui, Fatigue life prediction of engineering structures subjected to variable amplitude loading using the improved crack growth rate model, Fatigue & Fracture of Engineering Materials & Structures, 35 (2012) 278-290.
[14] J. Newman Jr, E. Anagnostou, D. Rusk, Fatigue and crack-growth analyses on 7075-T651 aluminum alloy coupons under constant-and variable-amplitude loading, International Journal of Fatigue, 62 (2014) 133-143.
[15] J. Willenborg, R. Engle, H. Wood, A crack growth retardation model using an effective stress concept, in, Air Force Flight Dynamics Lab Wright-Patterson Afb Oh, 1971.
[16] R. Branco, F. Antunes, J. Costa, A review on 3D-FE adaptive remeshing techniques for crack growth modelling, Engineering Fracture Mechanics, 141 (2015) 170-195.
[17] A. Loghin, U. Ozkan, A. Kaya, J. LeMonds, R. McClain, D. Decesare, S. Akkaram, J. Laflen, 3DFAS: framework for conducting 3D crack growth simulation, Propulsion-Safety Affordable Readiness, (2012).
[18] H. Pathak, A. Singh, I.V. Singh, Fatigue crack growth simulations of 3-D problems using XFEM, International Journal of Mechanical Sciences, 76 (2013) 112-131.

[19] S. Bhattacharya, I. Singh, B. Mishra, T. Bui, Fatigue crack growth simulations of interfacial cracks in bi-layered FGMs using XFEM, Computational Mechanics, 52 (2013) 799-814.
[20] F. Erdogan, G. Sih, On the crack extension in plates under plane loading and transverse shear, ASME. J. Basic Eng, 85(4) (1963) 519–525.
[21] M. Hussain, S. Pu, J. Underwood, Strain energy release rate for a crack under combined mode I and mode II, in: Fracture analysis: Proceedings of the 1973 national symposium on fracture mechanics, part II, ASTM International, 1974.
[22] S.K. Maiti, R. Smith, Comparison of the criteria for mixed mode brittle fracture based on the preinstability stress-strain field, International Journal of Fracture, 24 (1984) 5-22.
[23] J.D. Eshelby, The force on an elastic singularity, Philosophical Transactions of the Royal Society of London. Series A, Mathematical Physical Sciences, 244 (1951) 87-112.
[24] S.A. Silling, Reformulation of elasticity theory for discontinuities and long-range forces, Journal of the Mechanics and Physics of Solids, 48 (2000) 175-209.
[25] S.A. Silling, M. Epton, O. Weckner, J. Xu, E. Askari, Peridynamic states and constitutive modeling, Journal of Elasticity, 88 (2007) 151-184.
[26] S.A. Silling, R. Lehoucq, Peridynamic theory of solid mechanics, in: Advances in applied mechanics, Elsevier, 2010, pp. 73-168.
[27] S.A. Silling, E. Askari, A meshfree method based on the peridynamic model of solid mechanics, Computers & structures, 83 (2005) 1526-1535.
[28] E. Madenci, E. Oterkus, Peridynamic Theory and Its Applications, Springer, New York, 2014.
[29] E. Oterkus, I. Guven, E. Madenci, Fatigue failure model with peridynamic theory, in: 2010 12th IEEE Intersociety Conference on Thermal and Thermomechanical Phenomena in Electronic Systems, IEEE, 2010, pp. 1-6.
[30] S.A. Silling, A. Askari, Peridynamic model for fatigue cracking, SAND-18590. Albuquerque: Sandia National Laboratories, (2014).
[31] G. Zhang, Q. Le, A. Loghin, A. Subramaniyan, F. Bobaru, Validation of a peridynamic model for fatigue cracking, Engineering Fracture Mechanics, 162 (2016) 76-94.
[32] J. Jung, J. Seok, Mixed-mode fatigue crack growth analysis using peridynamic approach, International Journal of Fatigue, 103 (2017) 591-603.
[33] C.T. Nguyen, S. Oterkus, E. Oterkus, An energy-based peridynamic model for fatigue cracking, Engineering Fracture Mechanics, 241 (2020) 107373.
[34] L. Binchao, B. Rui, S. Fucheng, A fatigue damage-cumulative model in peridynamics, Chinese Journal of Aeronautics, 34 (2021) 329-342.
[35] G. Sarego, Q.V. Le, F. Bobaru, M. Zaccariotto, U. Galvanetto, Linearized state-based peridynamics for 2-D problems, International Journal for Numerical Methods in Engineering, 108 (2016) 1174-1197.
[36] C.T. Nguyen, S. Oterkus, Peridynamics for the thermomechanical behavior of shell structures, Engineering Fracture Mechanics, (2019) 106623.
[37] S.A. Silling, Linearized theory of peridynamic states, Journal of Elasticity, 99 (2010) 85-111.
[38] C. Diyaroglu, Peridynamics and its applications in marine structures, in, University of Strathclyde, 2016.
[39] J.T. Foster, S.A. Silling, W. Chen, An energy based failure criterion for use with peridynamic states, International Journal for Multiscale Computational Engineering, 9 (2011).
[40] E. Madenci, S. Oterkus, Ordinary state-based peridynamics for plastic deformation according to von Mises yield criteria with isotropic hardening, Journal of the Mechanics Physics of Solids, 86 (2016) 192-219.

[41] E. Madenci, S. Oterkus, Ordinary state-based peridynamics for thermoviscoelastic deformation, Engineering Fracture Mechanics, 175 (2017) 31-45.
[42] C.T. Nguyen, S. Oterkus, Peridynamics formulation for beam structures to predict damage in offshore structures, Ocean Engineering, 173 (2019) 244-267.
[43] C.T. Nguyen, S. Oterkus, Investigating the effect of brittle crack propagation on the strength of ship structures by using peridynamics, Ocean Engineering, 209 (2020) 107472.
[44] G.R. Irwin, Analysis of stresses and strains near the end of a crack traversing a plate, (1997).
[45] W. Guo, Three-dimensional analyses of plastic constraint for through-thickness cracked bodies, Engineering Fracture Mechanics, 62 (1999) 383-407.
[46] H. Voorwald, M. Torres, C.P. Júnior, Modelling of fatigue crack growth following overloads, International journal of fatigue, 13 (1991) 423-427.
[47] Z. Ding, X. Wang, Z. Gao, S. Bao, An experimental investigation and prediction of fatigue crack growth under overload/underload in Q345R steel, International Journal of Fatigue, 98 (2017) 155-166.
[48] Z. Ding, Z. Gao, X. Wang, Y. Jiang, Modeling of fatigue crack growth in a pressure vessel steel Q345R, Engineering Fracture Mechanics, 135 (2015) 245-258.
[49] Z. Gao, T. Zhao, X. Wang, Y. Jiang, Multiaxial fatigue of 16MnR steel, Journal of pressure vessel technology, 131 (2009).
[50] A.S.f.T.a.M. (ASTM), ASTM E647: standard test method for measurement of fatigue crack growth rates, American Society for Testing and Materials (ASTM), West Conshohocken, Pa, USA, 1999.